Specifications for Modelling Fuel Cell and Combustion-Based Residential Cogeneration Devices within Whole-Building Simulation Programs

A Report of Subtask B of
FC+COGEN-SIM
The Simulation of Building-Integrated
Fuel Cell and Other Cogeneration Systems

Annex 42 of the
International Energy Agency
Energy Conservation in Buildings and Community Systems Programme
First published: October 2007

REPORT EDITORS:
Nick Kelly (University of Strathclyde)
Ian Beausoleil-Morrison (Natural Resources Canada)

AUTHORED BY:
Ian Beausoleil-Morrison (Natural Resources Canada)
Alex Ferguson (Natural Resources Canada)
Brent Griffith (National Renewable Energy Laboratory)
Nick Kelly (University of Strathclyde)
François Maréchal (École Polytechnique Fédéral de Lausanne)
Andreas Weber (Swiss Federal Laboratories for Materials Testing and Research)

ANNEX 42 OPERATING AGENT:
Ian Beausoleil-Morrison (Natural Resources Canada)

ANNEX 42 SUBTASK B LEADER:
Nick Kelly (University of Strathclyde)

CITATION

Ian Beausoleil-Morrison (Natural Resources Canada), Andreas Weber (Swiss Federal Laboratories for Materials Testing and Research), François Maréchal (École Polytechnique Fédéral de Lausanne, Switzerland), Brent Griffith (National Renewable Energy Laboratory, USA), Alex Ferguson (Natural Resources Canada) and Nick Kelly (University of Strathclyde). Specifications for Modelling Fuel Cell and Combustion-Based Residential Cogeneration Device within Whole-Building Simulation Programs. A Report of Subtask B of FC+COGEN-SIM The Simulation of Building-Integrated Fuel Cell and Other Cogeneration Systems. Annex 42 of the International Energy Agency Energy Conservation in Buildings and Community Systems Programme. (111 pages).

Copies of this report may be obtained from the Annex 42 web site at: www.cogen-sim.net or from the IEA/ECBCS Bookshop at: www.ecbcs.org.

DISCLAIMER

Participating countries in ECBCS:
Australia, Belgium, CEC, Canada, Czech Republic, Denmark, Finland, France, Germany, Greece, Israel, Italy, Japan, the Netherlands, New Zealand, Norway, Poland, Portugal, Sweden, Switzerland, Turkey, United Kingdom and the United States of America.

ISBN No.: 978-0-662-47116-5
Catalogue No.: M154-14/3-2007E-PDF

Preface

International Energy Agency

The International Energy Agency (IEA) was established in 1974 within the framework of the Organisation for Economic Co-operation and Development (OECD) to implement an international energy programme. A basic aim of the IEA is to foster co-operation among the twenty-four IEA participating countries and to increase energy security through energy conservation, development of alternative energy sources and energy research, development and demonstration (RD&D).

Energy Conservation in Buildings and Community Systems

The IEA sponsors research and development in a number of areas related to energy. The mission of one of those areas, the ECBCS - Energy Conservation for Building and Community Systems Programme, is to facilitate and accelerate the introduction of energy conservation, and environmentally sustainable technologies into healthy buildings and community systems, through innovation and research in decision-making, building assemblies and systems, and commercialisation. The objectives of collaborative work within the ECBCS R&D programme are directly derived from the on-going energy and environmental challenges facing IEA countries in the area of construction, energy market and research. ECBCS addresses major challenges and takes advantage of opportunities in the following areas:

- exploitation of innovation and information technology;
- impact of energy measures on indoor health and usability;
- integration of building energy measures and tools to changes in lifestyles, work environment alternatives, and business environment.

The Executive Committee

Overall control of the programme is maintained by an Executive Committee, which not only monitors existing projects but also identifies new areas where collaborative effort may be beneficial. To date the following projects have been initiated by the executive committee on Energy Conservation in Buildings and Community Systems (completed projects are identified by (*)):

Annex 1: Load Energy Determination of Buildings (*)
Annex 2: Ekistics and Advanced Community Energy Systems (*)
Annex 3: Energy Conservation in Residential Buildings (*)
Annex 4: Glasgow Commercial Building Monitoring (*)
Annex 5: Air Infiltration and Ventilation Centre
Annex 6: Energy Systems and Design of Communities (*)
Annex 7: Local Government Energy Planning (*)
Annex 8: Inhabitants Behaviour with Regard to Ventilation (*)
Annex 9: Minimum Ventilation Rates (*)
Annex 10: Building HVAC System Simulation (*)

Annex 11: Energy Auditing (*)
Annex 12: Windows and Fenestration (*)
Annex 13: Energy Management in Hospitals (*)
Annex 14: Condensation and Energy (*)
Annex 15: Energy Efficiency in Schools (*)
Annex 16: BEMS 1- User Interfaces and System Integration (*)
Annex 17: BEMS 2- Evaluation and Emulation Techniques (*)
Annex 18: Demand Controlled Ventilation Systems (*)
Annex 19: Low Slope Roof Systems (*)
Annex 20: Air Flow Patterns within Buildings (*)
Annex 21: Thermal Modelling (*)
Annex 22: Energy Efficient Communities (*)
Annex 23: Multi Zone Air Flow Modelling (COMIS) (*)
Annex 24: Heat, Air and Moisture Transfer in Envelopes (*)
Annex 25: Real time HEVAC Simulation (*)
Annex 26: Energy Efficient Ventilation of Large Enclosures (*)
Annex 27: Evaluation and Demonstration of Domestic Ventilation Systems (*)
Annex 28: Low Energy Cooling Systems (*)
Annex 29: Daylight in Buildings (*)
Annex 30: Bringing Simulation to Application (*)
Annex 31: Energy-Related Environmental Impact of Buildings (*)
Annex 32: Integral Building Envelope Performance Assessment (*)
Annex 33: Advanced Local Energy Planning (*)
Annex 34: Computer-Aided Evaluation of HVAC System Performance (*)
Annex 35: Design of Energy Efficient Hybrid Ventilation (HYBVENT) (*)
Annex 36: Retrofitting of Educational Buildings (*)
Annex 37: Low Exergy Systems for Heating and Cooling of Buildings (LowEx) (*)
Annex 38: Solar Sustainable Housing
Annex 39: High Performance Insulation Systems
Annex 40: Building Commissioning to Improve Energy Performance
Annex 41: Whole Building Heat, Air and Moisture Response (MOIST-ENG)
Annex 42: The Simulation of Building-Integrated Fuel Cell and Other Cogeneration Systems (FC+COGEN-SIM)
Annex 43: Testing and Validation of Building Energy Simulation Tools
Annex 44: Integrating Environmentally Responsive Elements in Buildings
Annex 45: Energy Efficient Electric Lighting for Buildings
Annex 46: Holistic Assessment Tool-kit on Energy Efficient Retrofit Measures for Government Buildings (EnERGo)
Annex 47: Cost-Effective Commissioning for Existing and Low Energy Buildings
Annex 48: Heat Pumping and Reversible Air Conditioning
Annex 49: Low Exergy Systems for High Performance Buildings and Communities
Annex 50: Prefabricated Systems for Low Energy Renovation of Residential Buildings

Working Group - Energy Efficiency in Educational Buildings (*)
Working Group - Indicators of Energy Efficiency in Cold Climate Buildings (*)
Working Group - Annex 36 Extension: The Energy Concept Adviser (*)

(*) - Completed

Annex 42

The objectives of Annex 42 were to develop simulation models that advance the design, operation, and analysis of residential cogeneration systems, and to apply these models to assess the technical, environmental, and economic performance of the technologies. This was accomplished by developing and incorporating models of cogeneration devices and associated plant components within existing whole-building simulation programs. Emphasis was placed upon fuel cell cogeneration systems and the Annex considered technologies suitable for use in new and existing single and low-rise-multi-family residential buildings. The models were developed at a time resolution that is appropriate for whole-building simulation.

To accomplish these objectives Annex 42 conducted research and development in the framework of the following three Subtasks:

- Subtask A : Cogeneration system characterization and characterization of occupant-driven electrical and domestic hot water usage patterns.
- Subtask B : Development, implementation, and validation of cogeneration system models.
- Subtask C : Technical, environmental, and economic assessment of selected cogeneration applications, recommendations for cogeneration application.

Annex 42 was an international joint effort conducted by 26 organizations in 10 countries:

Belgium	• University of Liège / Department of Electrical Engineering and Computer Science • COGEN Europe • Catholic University of Leuven
Canada	• Natural Resources Canada / CANMET Energy Technology Centre • University of Victoria / Department of Mechanical Engineering • National Research Council / Institute for Research in Construction • Hydro-Québec / Energy Technology Laboratory (LTE)
Finland	• Technical Research Centre of Finland (VTT) / Building and Transport
Germany	• Research Institute for Energy Economy (FfE)
Italy	• National Agency for New Technology, Energy and the Environment (ENEA) • University of Sannio • Second University of Napoli
Netherlands	• Energy Research Centre Netherlands (ECN) / Renewable Energy in the Built Environment
Norway	• Norwegian Building Research Institute (NBRI) • Telemark University College
United Kingdom	• University of Strathclyde / Energy Systems Research Unit (ESRU)

	• Cardiff University / Welsh School of Architecture
United States of America	• Penn State University / Energy Institute • Texas A&M University / Department of Architecture • National Institute of Standards and Technology • National Renewable Energy Laboratory • National Fuel Cell Research Center of the University of California-Irvine
Switzerland	• Swiss Federal Laboratories for Materials Testing and Research (EMPA) / Building Technologies Laboratory • Swiss Federal Institute of Technology (EPFL)/ Laboratory for Industrial Energy Systems • Hexis AG (Hexis) • Siemens Switzerland AG (Siemens)

Acknowledgements

This report of Subtask B of Annex 42 was reviewed by:

- Morad Atif (National Research Council, Canada)
- Viktor Dorer (Swiss Federal Laboratories for Materials Testing and Research)
- Jürgen Gehrmann (Projektträger Jülich, Germany)
- Jean Lebrun (University of Liege, Belgium)

The assistance of the other participants of Annex 42 in producing this report is also gratefully acknowledged.

Nick Kelly

Subtask B Leader

Table of Contents

Introduction

This document contains the specifications for a series of residential cogeneration device models developed within IEA/ECBCS Annex 42.

The devices covered are: solid oxide and polymer exchange membrane fuel cells (SOFC and PEM), and internal combustion and Stirling engine units (ICE and SE).

These models have been developed for use within whole-building simulation programs and one or more of the models described herein have been integrated into the following simulation packages: ESP-r[1], EnergyPlus[2], TRNSYS[3] and IDA-ICE[4]

The models have been designed to predict the energy performance of cogeneration devices when integrated into a residential building (dwelling). The models account for thermal performance (dynamic thermal performance in the case of the combustion engine models), electrochemical and combustion reactions where appropriate, along with electrical power output. All of the devices are modelled at levels of detail appropriate for whole-building simulation tools.

The document is divided into three sections.

Section I outlines the background to the development of the models including:

- the technical requirements for the models;
- a summary review of existing cogeneration device models and;
- an overview of the common modelling strategy adopted within the Annex.

The section concludes with and recommendations on the use and further development of the models.

Sections II and III contain the detailed specifications for the fuel cell and combustion engine cogeneration models. Section II is dedicated to the SOFC and PEM fuel cell

[1] www.esru.strath.ac.uk

[2] www.eere.energy.gov/buildings/energyplus

[3] www.trnsys.com

[4] http://www.equa.se/ice

model descriptions. Section III details the ICE and SE models. Note that Sections II and III incorporate individual reports which do not share the same the same nomenclature.

Each specifications includes:

- a description and justification for the specific forms of model developed;
- a detailed description of all of the equations used within each model and;
- the model data requirements.

The model specifications in sections II and III are generic and will allow code developers outside Annex 42 to integrate the models into their own simulation programs.

Section I: Background

1 Annex 42 Technical Modelling Requirements

A primary focus of Subtask B of Annex 42 is the development of cogeneration system models for use within existing whole-building simulation programs. The models created by Annex 42 are being implemented into existing tools such as ESP-r, TRNSYS, and EnergyPlus. These cogeneration models can be used in conjunction with the simulation tools' existing capabilities (for modelling the building envelope, plant components, electrical systems, *etc*) to assess the technical, environmental, and economic performance of the residential cogeneration technologies.

The main requirement for the models developed within Annex 42 (from a user's perspective) is to accurately predict the thermal and electrical outputs of the residential cogeneration devices and their explicit interaction with the building's envelope, thermal plant, and electrical systems. Essentially, this means that the device models must interact with the other technical domains of the building simulation tool on a time-step basis. The need to rigorously model complex internal processes is less important (except where this has a direct bearing on the output of the model).

Additionally, the Annex 42 device models need to be of a form capable of being coupled to models of associated plant components, such as hot-water storage, peak-load boilers and heaters, circulating pumps and fans, radiators and air-handling units, *etc*. The inter-connection of these components will create systems models will in-turn be coupled to models that predict the building's thermal and electrical demands.

Typical uses for the component and associated integrated systems models developed include:

- Annual simulations for quantifying energy consumption and associated carbon emissions.
- Seasonal simulations where the objective is to analyse the performance of a building and systems over a particular subset of the year.

- Weekly simulations where the operation of the building and its systems is examined in more detail, analysing performance characteristics such as on/off cycling, over-heating and under-heating, response to significant daily variations in climate, and thermal comfort.
- Systems analysis simulations in which the performance of environmental systems is examined in fine detail, perhaps examining the transient performance with different operational settings, different component parameters or component configurations.

Consequently, the Annex 42 cogeneration models must also be capable of being used in simulations with significantly different objectives and operate with time-steps that are in the order of a few seconds to a few minutes and be suitable for conducting simulations over durations ranging from a day up to a year.

These technical requirements and constraints form the context for the development of the Annex 42 cogeneration models described in the Sections II and III.

2 Review of Existing Models

Prior to developing the cogeneration models needed to support activities within Annex 42, a review of existing cogeneration device models was undertaken (Kelly, 2004). This set out to identify existing simulation models of fuel cells and other small-scale cogeneration technologies that might be suitable and/or adaptable for use within the Annex. However, given the fact that residential cogeneration was a relatively new phenomenon and that it was evident prior to the review that only a small number of dedicated building simulation models existed, this review also examined other models published in the literature that had been used for engineering and scientific functions not related to building simulation. Subsequent to this initial review, other more device-specific literature searches were undertaken during the development of the individual model specifications.

The following sections summarise the outcomes of these reviews with regards to both fuel cells and combustion-based cogeneration devices.

2.1 Fuel Cells

Fuel Cell models at various levels of complexity were reviewed ranging from the very simple (Thorstensen [2001]) to the highly complex models, but with a limited focus (Petruzzi *et al*, [2003]). Most of these models were developed as stand-alone applications written in code such as C and were not intended for a simulation environment. These models focused on the detailed representation of the fuel cell's electrochemical processes while neglecting other components that comprise the system. There were very few references related to the modelling of the fuel cell within the context of a larger system.

Given the range of models available, Haraldsson and Wipke (2004) provided a useful classification scheme for PEMFC models, which was equally applicable to SOFC. They describe the approach of a model as either being theoretical (more commonly referred to as "mechanistic") or semi-empirical. Mechanistic models are based upon electrochemical, thermodynamic, and fluid dynamic relationships, whereas, the semi-empirical models rely mainly upon experimental data.

In addition to the different modelling approaches, very different levels of detail in models were also encountered. Spatial dimensions varied from zero to three. Zero-dimensional models operate with current-voltage (I-V) curves, whereas mechanistic models explicitly treat mass, momentum, and energy balances, and the electrochemical reactions; requiring the explicit definition of geometry.

Singhal and Kendall (2003) categorize the resolution of SOFC models in four levels: atomic/molecular, cell, stack, and system. Approaches at various levels of complexity can be used to produce coherent models for each of the levels. For example, a stack model could be produced using mechanistic approaches that solve mass, momentum, and energy balances and couple these to theoretical electrochemical relations to predict the cell's electrical and thermal performance. Alternatively, a stack model could be formed using an empirical I-V curve with a simple energy balance. As Singhal and Kendall (*ibid*) underline, the appropriate level of modelling resolution and approach depends upon the objectives of the modelling exercise.

It is important to underline that the scope of the vast majority of the (non-systems simulation) fuel cell models reviewed was too limited or narrow in focus for the purposes

of Annex 42. Many of these models focus on single cells or stacks of cells while other components (e.g. afterburner, reformer) are left untreated (e.g. Beale et al 2003; Bove et al 2005). Other models (e.g. Van herle et al 2004) focus on system design aspects and balance of plant without considering the part load operation and the dynamic behaviour of the complete system.

Of the very few fuel cell models developed specifically for building or systems simulation, Ferguson and Ugursal (2002), Braun (2002) (who extracted a systems-simulation-compatible model from a more detailed mechanistic model), and Beausoleil-Morrison et al. (2002) provide a good practical basis for further model development. However, in these models and others, the dynamics of the fuel cell and associated balance of plant were rarely considered, particularly dynamics associated with thermal mass. This could be important in certain simulation contexts (e.g. detailed analysis of load matching control strategies) given that thermal transients of several minutes can be encountered in both the thermal and electrical performance of fuel cells.

It was concluded that none of the models reviewed were suitable candidates for inclusion into building simulation tools: all have some form of shortcoming such as a lack of validation, incomplete modelling of some aspect of performance, over-complexity, over-simplification, etc. This finding is not surprising given the relative immaturity of fuel cell modelling, and small number of models, particularly in the field of small-scale fuel cells (<10kW). These findings concur with those of Braun (*ibid*).

It was concluded that Annex modelling work would need to focus on the development of fuel cell models that had a level of complexity appropriate to whole-building simulation tools and which accounted for the relevant physical phenomena (i.e. heat *and* power), which could be encountered in the analysis of residential energy systems.

2.2 Combustion Engine Models

The review of the literature revealed that there had been few attempts to model combustion engine based small and micro-scale cogeneration in building simulation tools. McRorie *et al*. (1996) describe a partial model of an internal combustion engine that might be used in systems level simulations; however in the state described in the paper the model could not be fully integrated into building simulation codes without

considerable effort. Kelly (1998) incorporated a multi-component small-scale engine model into the ESP-r building simulation tool. The parameters derived for the model were taken from tests on a 2-cylinder diesel engine unit — an atypical example of the genre. Pearce *et al*. (1996, 2001) studied the annual performance of Stirling engines in comparison to measured and calculated residential heating loads by assuming constant, seasonal efficiencies, This modelling approach neglected the effects of different control strategies and thermal storage, which are of interest when investigating the integration of this technology in residential buildings. None of the models were deemed particularly suitable for use within Annex 42.

Nevertheless, the literature is rich with Stirling engine (SE) and internal combustion engine (ICE) models developed for general (as opposed to cogeneration -specific) analysis. (eg. Dochat 1993, Heywood 1998). These models vary considerably in their approach and resolution; Urieli and Berchowitz (1984) classify them into three categories:

- *First-order* models use thermodynamic principles to characterize engine performance in steady-state operation.
- *Second-order* models divide an engine's working fluid into one or more control volumes, and characterize the system's dynamic performance at discrete, sub-cycle time steps.
- *Third-order* models further divide the piston-cylinder configuration into additional control volumes suitable for finite-element analysis.

Urieli and Berchowitz (*ibid*) omitted a fourth class of engine model from their categorization — parametric, or *zero-order* models that rely entirely on empirical data and make no attempt to characterize the thermo-physical processes occurring within the system.

The majority of the engine models available in the literature fell into the last two categories and had been developed for the analysis of engine phenomena occurring over very short time scales (10^{-3} to 10^{-6} seconds). As Building simulation operates using time scales many orders of magnitude longer (~10 to 10^{3} seconds). The combination of the

two groups of models is impractical, as solving the resulting set of excessively stiff[5] equations would be difficult if not impossible using the numerical solution techniques currently employed in simulation tools.

Moreover, many of the processes characterised by the engine models reviewed (e.g. the variation of thermodynamic properties within a cylinder during a single engine stroke [Abd Alla, 2002]) are simply not relevant within the context of building simulation, where it is the thermal and electrical output, fuel consumption, dynamic thermal transients and heat recovery from the engine that are of interest.

Again, from the review it was concluded that modelling work would need to focus on the development of system-simulation-compatible engine models that adequately represented the thermal, chemical and electrical phenomena necessary for dynamic simulations involving models of cogeneration, balance of plant and the building envelope.

3 Annex 42 Modelling Strategy (Modelling approach)

Taking account of the modelling requirements outlined in Section 2, specifically the need for integration within a wider systems simulation, tends to exclude the development or adaptation of very detailed fuel cell or combustion engine models, where the level of detail in the modelling of the component is far greater than the building and systems model into which it would be integrated. Further, the data burden associated with using the model could be prohibitive and any benefit in terms of accuracy of results obtained from such a model could be lost when coupling the output to simpler models that would provide its boundary conditions. Moreover, a criticism often levelled at detailed simulation models is that much of the data required to run them in unobtainable other than by very detailed laboratory tests.

A pragmatic “grey box” approach was adopted in the development of the fuel cell and combustion engine component models. In grey box models, the model structure reflects a partial-knowledge of the underlying system, however the form and parameters for the individual model equations describing the associated physical processes can be derived

[5] Equations describing phenomena with vastly differing time constants.

from comparison with easily obtainable empirical data or extracted from more detailed models.

Ferguson (2005), describes two different approaches to grey box modelling of Stirling engine units that are applicable to the modelling of all cogeneration devices: a "sub-system" approach and "systems-level" (or single component) approach – effectively describing the device using multiple and single control volumes respectively. In the former the device is broken down into functional components (e.g. heat exchanger) each component is then described using a "control volume", the physical processes of which are described using one or more parametric equations. In the latter the engine unit is represented as a single functional block with a series of inputs and outputs, these are linked by a performance map of the unit: this being a series of parametric equations linking the inputs of the model to the outputs, the coefficients of these equations being determined by lab testing of the component and calibration. Both approaches are equally applicable to the modelling of an ICE unit, and both have their merits and drawbacks.

The popularity of the grey box modelling approach is evidenced by its extensive use in many different branches of engineering and science. For example, Clarke (2001) describes a grey box model of a boiler, while Hrovat and Sun (1997) describe a multi-component engine model, where the individual components are described by parametric equations.

The models described in Sections II and III, while exhibiting different levels of knowledge of the underlying system consistently use the grey box approach.

4 Comments on the Use of Models and Future Work

4.1 Limits to Validity

As has been mentioned previously, the models described in sections II and III are intended for use by the wider building simulation community and have been derived from literature review, lab and field-testing of devices. The models are intended for use in energy systems simulations and at time steps appropriate to that field: 1 second up to a few minutes. Note that it is not recommended to use these models with half-hourly or hourly time steps as their accuracy could be compromised.

Given that the models could be applied to a wide variety of cogeneration devices, they have been designed with considerable flexibility in mind (a feature inherent in the grey box modelling approach). The forms of the models are therefore applicable to almost any PEM, SOFC or combustion engine device if re-calibration is undertaken. However, the parameters required to define the governing equations can be determined from bench testing of cogeneration devices.

In the case of the combustion engine model, non-intrusive measurements (e.g. fuel flow rate, cooling water flow rates and temperature, electrical production) are sufficient to calibrate the model. Due to its more detailed nature, some intrusive measurements (e.g. gas temperature flowing into gas-to-water heat exchanger, DC power flowing into power converter, air supply rate) are required to calibrate the fuel cell model.

The ability to re-use and recalibrate the component models or sub-models should ensure that they are applicable to future generations of cogeneration devices: which is important in the case of such a rapidly changing technology field.

4.2 Future Work

While the combustion engine models account for thermal transient effects in cooling water outlet temperature, the SOFC and PEM models currently only calculate the steady-state performance at a particular simulation time step. However a similar approach to that adopted in the combustion engine models could equally be applied to the fuel cell models: where extra, massive thermal control volumes are associated with the cooling water heat exchangers.

Finally, while all of the models calculate CO_2 emissions, other pollutant emissions such as SO_x and NO_x are not dealt with in detail. The combustion engine models incorporate a form of equation suitable for the modelling of time-varying non-CO_2 pollutant emissions, however no attempt has been made to calibrate and validate these equations.

5 References

Abd Alla, G H. (2002) “Computer simulation of a four stroke spark ignition engine”, Energy Conversion and Management, 43, pp1043-106.

Beale S.B., Lin Y., Zhubrin S.V., and Dong W. (2003), "Computer Methods for Performance Prediction in Fuel Cells", *J. Power Sources* (118) 79-85.

Beausoleil-Morrison I., Cuthbert D., Deuchars G., and McAlary G. (2002), “The Simulation of Fuel Cell Cogeneration Systems within Residential Buildings”, *Proc. eSim 2002*, 40-47, The Canadian Conference on Building Energy Simulation, Montréal Canada.

Bove R., Lunghi P., and Sammes N.M. (2005), "SOFC Mathematical Model for Systems Simulations. Part 1: From a Micro-Detailed to Macro-Black-Box Model", *Int J Hydrogen Energy* (30) 181-187.

Braun R, (2002), Optimal Design and Operation of Solid Oxide Fuel Cell Systems for Small-Scale Stationary Applications, PhD Thesis, University of Wisconsin-Madison.

Clarke J A, 2001, *Energy Simulation in Building Design*, 2nd Ed, Butterworth Heinemann, London.

Dochat, G. 1993. , SPDE/SPRE final summary report, Technical report, Mechanical Technology Incorporated.

A. Ferguson A, and Ugursal V I, Fuel cell modelling for building cogeneration applications, Journal of Power Sources 137 (2004) (1), pp. 30–42.

Ferguson A, 2005, Stirling Engine model specifications, IEA Annex 42 draft internal report.

Haraldsson K and Wipke K (2004), "Evaluating PEM Fuel Cell System Models", Journal of Power Sources, 126, pp88-97.

Heywood J B, 1998, Internal Combustion Engine Fundamentals, McGraw Hill.

Hrovat D and Sun J, "Models and Control Methodologies for IC Engine Idle Speed Control Design," IEE Control Engineer Practice, Issue 5, pp. 1093-1100, August, 1997.

Kelly N J (1998), Towards a design environment for building-integrated energy systems: the integration of electrical power flow modelling with building simulation, PhD thesis, University of Strathclyde.

Kelly N J, 2004, Review of small scale cogeneration system models, IEA Annex 42 draft internal report.

McRorie K A B, Underwood C P, Le Feuvre R F (1996), "Small Scale Combined Heat and Power Simulations: Development of a Dynamic Spark Ignition Engine Model", Building Services Research and Technology 17(3), pp153-159.

Pearce, J., Al Zahawi, B., Aukland, D. Starr, F. (1996), 'Energy generation in the home: evaluation of single-house domestic combined heat and power', IEE Proceedings of Science, Measurement and Technology 143(6), pp345–350.

Pearce, J., Al Zahawi, B. Shuttleworth, R. (2001), 'Energy generation in the home: modelling of single-house domestic combined heat and power', IEE Proceedings of Science, Measurement and Technology 148(5), pp197–203.

Petruzzi L, S Cocchi and F Fineschi F, 2003, A Global Chemical Model for SOFC Systems Design and Engineering, Journal of Power Sources, 118, pp96-107.

Thorstensen B, 2001, A parametric Study of Fuel Cell System Efficiency under Full and Part Load Operation, Journal of Power Sources, 92, pp9-16.

Singhal S.C. and Kendall K. (2003), High Temperature Solid Oxide Fuel Cells: Fundamentals,Design, and Applications, Elsevier, Oxford UK.

Urieli, I. Berchowitz, D. (1984), Stirling cycle analysis, Adam Hilger Ltd. Bristol.

Van herle J., Maréchal F., Leuenberger S., Membrez Y., Bucheli O., and Favrat D. (2004), "Process Flow Model of Solid Oxide Fuel Cell System Supplied with Sewage Biogas", *J. Power Sources* (131) 127-141.

Section II: Fuel Cell Cogeneration Model Specifications

Specifications for Modelling Fuel Cell Cogeneration Devices within Whole-Building Simulation Programs

MODEL SPECIFICATION AUTHORS:

Ian Beausoleil-Morrison (Natural Resources Canada)

Andreas Weber (Swiss Federal Laboratories for Materials Testing and Research)

François Maréchal (École Polytechnique Fédéral de Lausanne, Switzerland)

Brent Griffith (National Renewable Energy Laboratory, USA)

Acknowledgements

The authors of this report would like to acknowledge the contributions of the following individuals:

- Adrian Schatz (Formerly with Sulzer-Hexis Ltd.)
- Ismet Ugursal (Dalhousie University, formerly with University of Victoria)
- Conrad Gähler (Siemens Building Technologies Ltd.)
- Viktor Dorer (Swiss Federal Laboratories for Materials Testing and Research)
- Gordon McAlray (Formerly with FCT Ltd.)
- Gord Deuchars (Formerly with FCT Ltd.)
- Adam Tuck (Formerly with FCT Ltd.)
- Matt Hofford (Formerly with FCT Ltd.)
- Sébastien Lerson (Formerly with University of Liège)

The assistance of the other members of Annex 42 in producing this report is also gratefully acknowledged.

1. Modelling Approach

The fuel cell cogeneration (FC-cogeneration) model described in this specification will be coupled to models of associated plant components, such as hot-water storage, peak-load boilers and heaters, pumps that circulate hot or cold water from the plant to hydronic heaters located in the rooms or to air-handling units, fans that circulate conditioned air to the rooms, and heat exchangers. In turn, the models of the coherent systems will be coupled to models that predict the building's thermal and electrical demands.

Given these objectives (and the constraints they impose), an assemblage of models of the following subsystems, each represented by a control volume, is used to simulate the performance of the complete FC-cogeneration system:

- The fuel cell power module.
- The air supply blower.
- The fuel supply compressor (if present).
- A water pump (if required for steam reformation).
- An auxiliary burner (if present upstream of the exhaust-gas-to-water heat exchanger).
- An exhaust-gas-to-water heat exchanger.
- A battery system for electrical storage.
- A power conditioning unit (PCU) for converting the fuel cell's DC electrical output to AC.
- A dilution air system (if present downstream of the gas-to-water heat exchanger) with optional heat recovery ventilator (HRV).
- A heat exchanger in the stack cooling system
- An air cooler in the stack cooling system
- A stack cooling circuit pump

The energy flows between these twelve subsystems are illustrated schematically in Figure II-1. The control volumes representing each of these subsystems and the proposed modelling methods are elaborated in the following sections. A numbering scheme representing the state points of the fluids entering and exiting the control volumes is presented in Figure II-2.

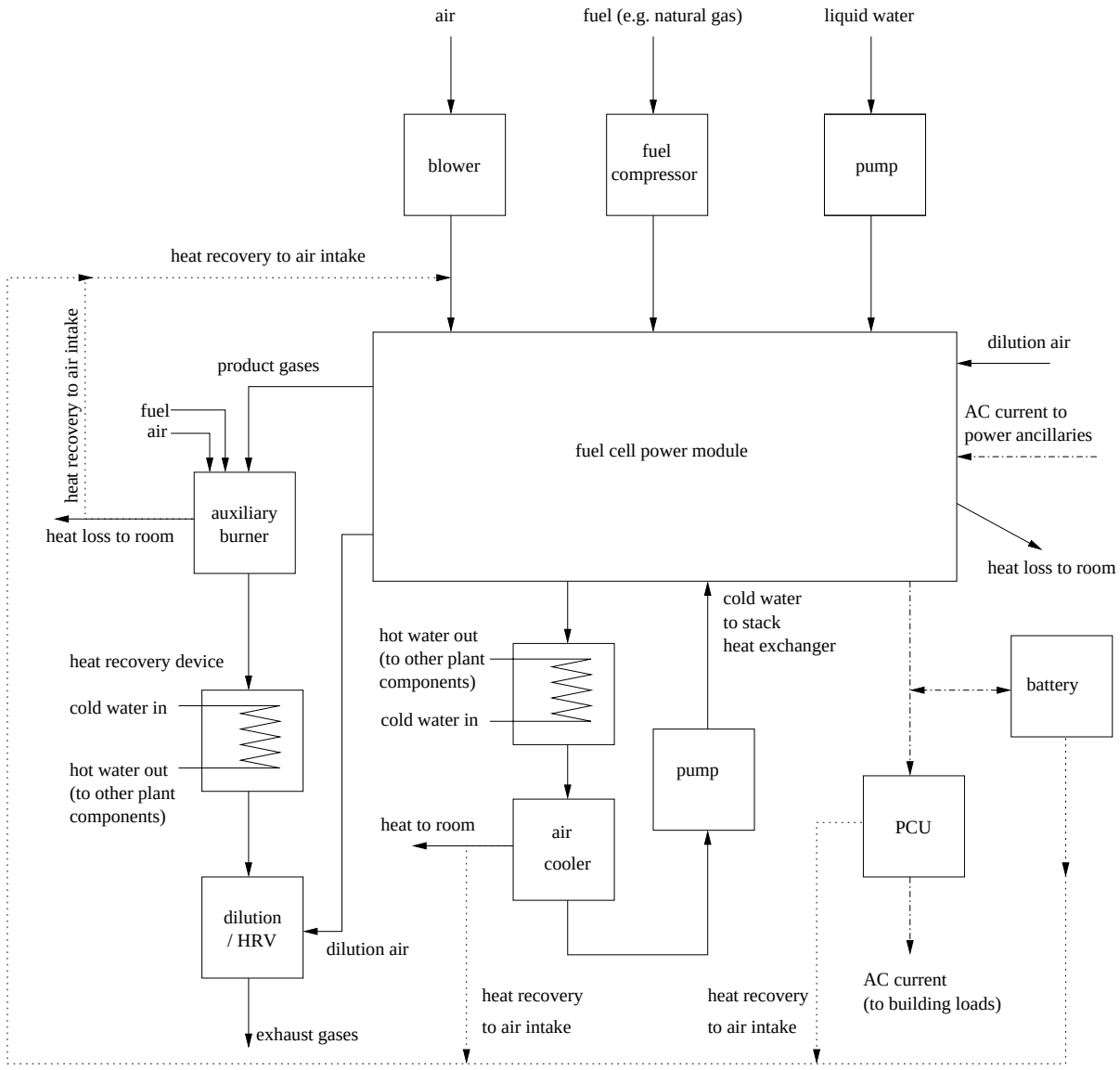

Figure II-1: Schematic of energy flows between FC-cogeneration device's subsystems

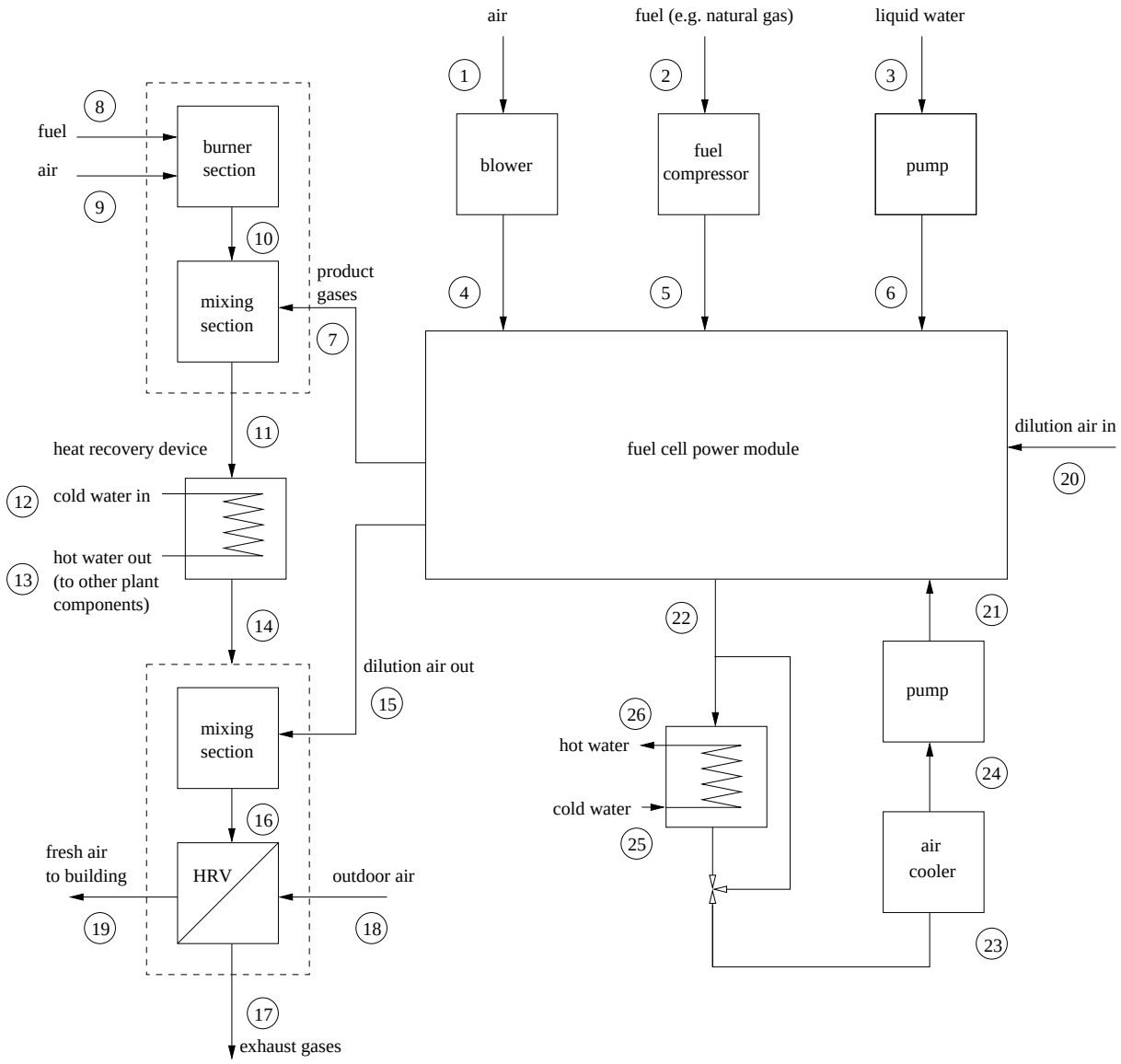

Figure II-2: State point numbering scheme for fluids entering and exiting control volumes

2. Fuel Cell Power Module

The control volume representing the fuel cell power module (FCPM) represents much more than the fuel cell stack. The following devices are included within this control volume:

- The fuel cell stack, which includes the electrodes, the electrolyte, interconnects, fuel and air channels, internal heat exchanger, etc.
- The fuel pre-heater, fuel desulfurizer (if present), fuel reformer, pre-reformer, steam reformer, shift reactors, valves and actuators that control the flow of fuel, but not the fuel compressor (if present).
- The air filter and pre-heater, but not the blower which pressurizes the air.
- The afterburner or combustor downstream of the stack that combusts unreacted fuel.
- The water preparation system, but not the pump which supplies the water (if required for steam reformation).
- Central controllers and any other power consuming ancillaries not specifically included in the other control volumes.

Figure II-3 illustrates one possible arrangement of a FCPM with the above-mentioned components.

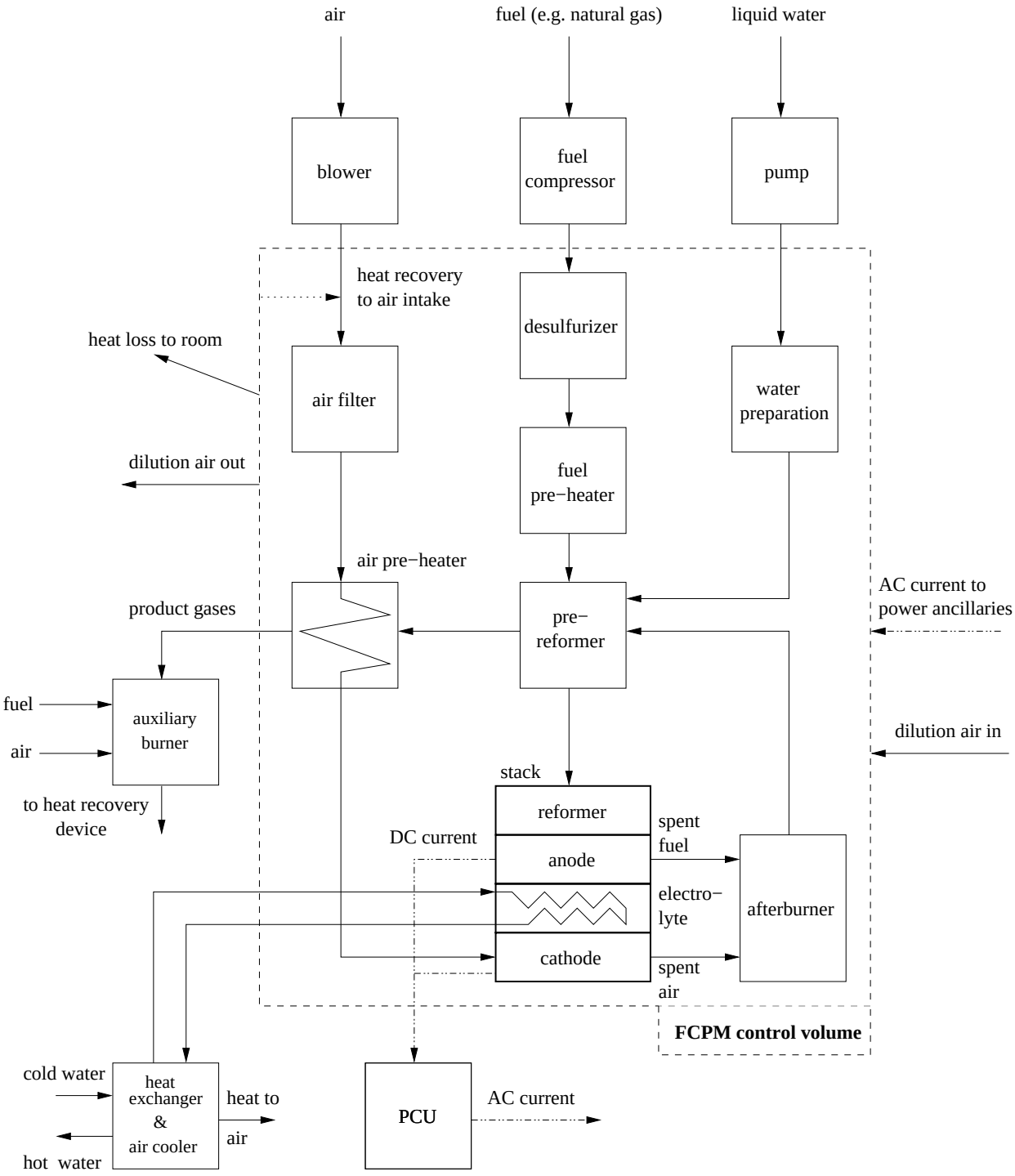

Figure II-3: Schematic of one possible arrangement of components within FCPM control volume

The FCPM control volume is drawn to encompass the above-mentioned components for a number of pragmatic reasons:

- Product-specific information regarding the arrangement of components such as afterburners and pre-heaters is not required, an important consideration since many manufacturers consider this information to be proprietary.
- The model can represent SOFC's with external reforming (via coupling to a separate reformer model), indirect internal reforming (hydrocarbons are reacted to H_2 and CO at a catalyst that is physically separated but thermally coupled to the anode), or direct internal reforming (hydrocarbons are reacted at the anode). It can also represent SOFC's that are supplied with hydrogen rather than hydrocarbon fuels.
- The model can represent both planar and tubular SOFC designs.
- The model can represent both hydrocarbon-fed PEMFC units (including the reformer) or hydrogen-fed PEMFC units.
- Inputs to the model can be derived from empirical measurements made on either individual subsystems or from coherent system testing. Alternatively, the input data required to characterize this control volume can be derived from highly detailed mechanistic subsystem modelling that is performed independently from the building simulation programs.

Various aspects of the FCPM model are treated in the following subsections.

2.1 Energy balance

Referring to the control volume in Figure II-3 (the dashed line), an energy balance can be written for the control volume representing the FCPM as follows,

$$\dot{H}_{fuel} + \dot{H}_{air} + \dot{H}_{liq-water} + \dot{H}_{dilution-air-in} + P_{el,ancillaries-AC} \qquad \text{(II-1)}$$

$$= P_{el} + \dot{H}_{FCPM-cg} + q_{s-cool} + q_{skin-loss} + \dot{H}_{dilution-air-out}$$

Where $\dot{H}_{air}$ is the total enthalpy flow rate of the air introduced to the control volume, that is downstream of the blower (W). Similarly, $\dot{H}_{fuel}$ is the total enthalpy flow rate of the fuel introduced to the control volume, that is downstream of the fuel compressor (W). $\dot{H}_{liq-water}$ is the total enthalpy flow rate of the liquid water, if required for steam reformation, introduced to the control volume, that is downstream of the water pump (W). $\dot{H}_{FCPM-cg}$ is the total enthalpy flow rate of the product gases that exit the control volume and enter the auxiliary burner (W). These result from the electrochemical and combustion reaction of the fuel and air as well as the water vapour that results from the supply of liquid water for steam reformation. q_{s-cool} is the heat to be

extracted from the stack by the stack cooling system in order to control the temperature in a PEMFC stack (W). $q_{skin-loss}$ are the parasitic thermal losses from the control volume in the form of radiation and convection to the containing room (W).

In equation II-1 P_{el} is the net DC electric power (W) produced by the FCPM, that is the power produced by the fuel cell stack less the power draw of the ancillaries that are included within the control volume and that are powered directly by the fuel cell's DC output. $P_{el,ancillaries-AC}$ is the power draw of the ancillaries that are included within the control volume and that are powered by AC electricity that is supplied to the cogeneration device. This treatment does not double count for the power draw of the ancillaries, but rather provides flexibility in its representation, this to reflect the possible design configurations. In some cases the ancillaries (e.g. controls, pumps, fans) may be powered directly by the fuel cell's DC output, while in other cases the ancillaries may be supplied by AC power from the grid.

$\dot{H}_{dilution-air-in}$ and $\dot{H}_{dilution-air-out}$ in equation II-1 represent the total enthalpy flow rates of air that is drawn through the cabinet for cooling purposes and subsequently added to the the dilution air system/HRV control volume. This feature is not used in all FC-cogeneration devices.

For the gas streams (inlet air and fuel; product gases) the total enthalpy terms in equation II-1 represent summations of the enthalpies of their constituent gases,

$$\dot{H}_{fuel} = \sum_i (\dot{N}_i \hat{h}_i)_{fuel} \tag{II-2}$$

$$\dot{H}_{air} = \sum_i (\dot{N}_i \hat{h}_i)_{air} \tag{II-3}$$

$$\dot{H}_{FCPM-cg} = \sum_i (\dot{N}_i \hat{h}_i)_{FCPM-cg} \tag{II-4}$$

Where $\hat{h}_i$ is the molar enthalpy (J/kmol) and $\dot{N}_i$ is the molar flow rate (kmol/s) of gas constituent *i*. Each of equations II-2 through II-4 are summed over the gases that form the stream. For example, the fuel stream may be composed of hydrogen (H_2), hydrocarbons, and non-combustibles.

Since chemical reactions are occurring within the FCPM, equations II-2 through II-4 are evaluated using standardized enthalpies. This ensures that the enthalpy of each reactant or product gas is properly related to the enthalpies of other elements and compounds by using a standard reference state. By convention, the standard state is taken to be 25°C and 1 atmosphere pressure and the enthalpies of all elemental substances (e.g. O_2, H_2) are taken to be zero at the standard state.

For convenience, the enthalpy of each reactant or product gas is expressed as a sum of its enthalpy at the standard state (i.e. the standard enthalpy of formation) and the deviation between

its enthalpy and that at the standard state,

$$\hat{h}_i = \Delta_f \hat{h}_i^o + \left[\hat{h}_i - \Delta_f \hat{h}_i^o \right] \tag{II-5}$$

Where $\Delta_f \hat{h}_i^o$ is the molar enthalpy of gas *i* at the standard state (J/kmol).

If it is assumed that the reactions of the hydrocarbon and/or hydrogen fuel are complete (refer to the discussion in subsection 2.8), then the fuel's lower heating value can be conveniently introduced into the energy balance. The lower heating value of a fuel is expressed using the standard enthalpies of formation of the reactants and products (see, for example, Reynolds and Perkins 1977),

$$LHV_{fuel} = \frac{\Delta_f H_{fuel}^o + \Delta_f H_{O_2}^o - \Delta_f H_{CO_2}^o - \Delta_f H_{H_2O}^o}{\dot{N}_{fuel}} \tag{II-6}$$

$$= \frac{\Delta_f H_{fuel}^o - \Delta_f H_{CO_2}^o - \Delta_f H_{H_2O}^o}{\dot{N}_{fuel}}$$

Where $\Delta_f H_{fuel}^o$ is the total flow rate of the standard enthalpy of formation of the fuel entering the FCPM control volume (W). $\Delta_f H_{CO_2}^o$ and $\Delta_f H_{H_2O}^o$ and the total flow rates of the total enthalpies of formation of the product gases created by the complete reaction of the fuel (W). $\dot{N}_{fuel}$ is the molar flow rate of the fuel (kmol/s) and LHV is the lower heating value of the fuel (J/kmol).

It is important to note that the $\Delta_f H_{H_2O}^o$ term in equation II-6 pertains only to the water vapour created through the electrochemical and combustion reaction of the fuel and oxygen. The water vapour that appears in the product gases as a result of the liquid water supplied for steam reformation is not considered in this term. (The reaction of this liquid water is treated in subsection 2.8).

However, the water vapour generated from steam reformation is included in the term $\dot{H}_{FCPM-cg}$ in equation II-1. By representing the enthalpy of the liquid water supply with equation II-5 and by grouping the standard enthalpy of formation of the water vapour associated with the reforming water with the liquid enthlapy term, it can be shown that

$$\dot{H}_{liq-water} - \left(\dot{N} \Delta_f \hat{h}^o \right)_{H_2O,vap} = \dot{N}_{liq-water} \left(\Delta_f \hat{h}_{H_2O,liq}^o + \left[\hat{h} - \Delta_f \hat{h}^o \right]_{H_2O,liq} - \Delta_f \hat{h}_{H_2O,vap}^o \right) \tag{II-6a}$$

$$= \dot{N}_{liq-water} \left(\left[\hat{h} - \Delta_f \hat{h}^o \right]_{H_2O,liq} - \Delta_f \hat{h}_{H_2O,fg}^o \right)$$

Where $\dot{N}_{liq-water}$ is the molar flow rate of liquid water (kmol/s) added for reformation purposes.

(Subsection 2.8 will demonstrate that this is also equal to the augmentation of flow rate of water vapour exiting the FCPM control volume as a result of the liquid water supply.) $\Delta_f \hat{h}^o_{H_2O,\,fg}$ is the latent heat of vapourization of water at the standard state (J/kmol).

Substituting equations II-2 through II-6a into equation II-1 leads to the following form of the energy balance of the FCPM control volume,

$$\sum_i (\dot{N}_i \cdot [\hat{h}_i - \Delta_f \hat{h}^o_i])_{fuel} + \sum_i (\dot{N}_i \cdot [\hat{h}_i - \Delta_f \hat{h}^o_i])_{air} \tag{II-7}$$

$$+ \dot{N}_{liq-water}\left(\left[\hat{h} - \Delta_f \hat{h}^o\right]_{H_2O,liq} - \Delta_f \hat{h}^o_{H_2O,\,fg}\right) + \dot{H}_{dilution-air-in} + \dot{N}_{fuel} \cdot LHV_{fuel} + P_{el,ancillaries-AC}$$

$$= P_{el} + \sum_i (\dot{N}_i \cdot [\hat{h}_i - \Delta_f \hat{h}^o_i])_{FCPM-cg} + q_{s-cool} + q_{skin-loss} + \dot{H}_{dilution-air-out}$$

The methods used to evaluating the various terms of equation II-7 are treated in the following subsections.

2.2 Electrical efficiency

It is common to model the electrochemical behaviour of fuel cell stacks by predicting cell voltages using the Nernst potential with empirical adjustments to account for activation, concentration, and ohmic losses (see for example Bove et al 2005; Chan and Ding 2005). Such an approach requires methods to establish the stack temperature and stack fuel utilization efficiency. This can only be accurately accomplished with an a priori knowledge of the system configuration and operational controls and introduces numerous assumptions regarding the heat transfer characteristics between individual components.

As elaborated in Section 2 the fuel cell stack has been grouped with other components such as the afterburner, heat exchangers, and fuel processing into the FCPM control volume. Such a treatment avoids the complications discussed above but also precludes an explicit treatment of the fuel cell's electrochemical behaviour. Consequently, this model does not attempt to simulate the electrochemical processes occurring within the fuel cell, but rather represents the electrochemical performance of the FCPM using a parametric relation between the electrical efficiency and the net electrical power output. This is given as,

$$\varepsilon_{el} = \left[\varepsilon_0 + \varepsilon_1 \cdot P_{el} + \varepsilon_2 \cdot P_{el}^2\right] \cdot \left[1 - N_{stops} \cdot D\right] \cdot \left[1 - MAX\left|\int_0 dt - t_{threshold}\ ,\ 0\right| \cdot L\right] \tag{II-8}$$

As previously defined, P_{el} is the net DC electric power (W) produced by the FCPM, that is the

power produced by the fuel cell stack (P_{gross}) less the power draw of the ancillaries that are included within this control volume and that are powered directly by the fuel cell's electrical output,

$$P_{el} = P_{gross} - P_{el,ancillaries-DC} \tag{II-9}$$

ε_{el} is the electrical efficiency of the FCPM and is defined as the net DC power output from the FCPM relative to the fuel's LHV,

$$\varepsilon_{el} = \frac{P_{el}}{\dot{N}_{fuel} \cdot LHV_{fuel}} \tag{II-10}$$

The $[1 - N_{stops} \cdot D]$ term in equation II-8 represents the degradation of the FCPM's electrical efficiency as a result of stop-start cycling. (Due to their high operating temperatures and the thermal stresses that may be experienced during system cool-down and warm-up periods, the fuel cell's electrical performance may degrade with time.) N_{stops} represents the number of times the SOFC-cogeneration system has been stopped and then restarted since its initiation and D is a user-input fixed value representing the fractional performance degradation associated with each cycle. System start and stop periods are further discussed in subsection 2.4.

The "L" term in equation II-8 represents the degradation of the FCPM's electrical efficiency as a result of operational degredation. The time integral represents the accumulated time of operation from the initial system start. L is a user-input fixed value representing the fractional performance degredation associated with operating time. $t_{threshold}$ is a user-input fixed time value which can be used to represent systems that may show no degradation for a period of time ($t_{threshold}$), but degrade thereafter.

The approach represented by equations II-8 through II-10 will provide the Annex 42 model with a great deal of flexibility to deal with various techniques for characterizing a FCPM's electrochemical performance. The ε_i required by equation II-8 are supplied by the user. These coefficients could be determined by regressing measured data from a coherent system. Alternatively, empirical or analytical models could be used to predict polarization curves for a given cell design, and additional models coupled to these to predict fuel utilization ratios and flow rates to produce a performance map that leads to the ε_i coefficients. Another option is to employ detailed multi-dimensional (one to three) mechanistic electrochemical, flow, and energy models based upon numerical discretization and solution schemes to predict FCPM performance over a range of operating points and then parameterize the results to yield the ε_i coefficients. Examples of detailed models that could be used are those of Braun (2002) and Petruzzi et al (2003). Other potential models are described by Kelly (2004). It is worth noting that the three options listed above for establishing the ε_i coefficients all rely heavily upon empirical data, either

characterizing performance at the system level or at the molecular level.

It is felt that a second order parametric is sufficient in equation II-8 for characterizing the performance over a FCPM's range of operation, but higher-order terms can easily be added if necessary.

2.3 Electrical system control behaviour

Beausoleil-Morrison et al (2002) included the PCU and battery inside the FCPM control volume. Whereas, these devices are located outside the FCPM control volume in the Annex 42 model, this to enable the study of issues such as electrical storage, SOFC transient behaviour, and power conditioning. This approach necessitates assumptions regarding the control behaviour between these components. It must be recognized that the design of control systems is likely to be regarded as proprietary by many manufacturers. Therefore, in modelling real systems the user is likely to collapse the behaviour of the PCU and battery within the electrical efficiency relationship (equation II-8), effectively nullifying the PCU and battery control volumes. Notwithstanding, the model is structured in this way to enable research on the sensitivity of system performance to PCU and battery characteristics and to allow the analysis of hypothetical systems.

The model will impose the following control behaviour:

- A controller external to the FC-cogeneration model will apply some control logic (some possibilities are given by Ferguson 2004) to demand a net AC electrical output from the FC-cogeneration device for the current simulation time-step, P_{demand}.
- The AC draw required to power the FCPM's and other control volumes' ancillary devices will be determined, $P_{AC-ancillaries-total}$. (Refer to subsection 2.9 and Sections 3, 4, 5, 6, and 9 for the treatment these AC-powered ancillaries.) This will be added to P_{demand} to determine the gross AC output from the PCU that is required to supply a net of P_{demand} from the FC-cogeneration device, $P_{gross-demand} = P_{demand} + P_{AC-ancillaries-total}$.
- The model of the PCU will account for the losses associated with power conditioning ($P_{PCU-losses}$) to supply this demand and thus establish the required DC output from the FCPM and/or battery, $P_{gross-demand} + P_{PCU-losses}$. (This may require iteration.)
- Subject to this demand, the user-specified operating range for the DC electrical output (P_{el-min} and P_{el-max}), and its transient operational constraints (treated in Section 2.4), the FCPM's operating point for the current time-step will be established, P_{el}.
- If the FCPM's operating point results in a deficit of power (i.e. $P_{el} < P_{demand} + P_{PCU-losses}$) then the battery will attempt to supply the required additional power to the PCU. Subject to its operational constraints (treated in Section 10), the battery's response will be determined, $P_{battery-discharge}$.

- If the FCPM's operating point results in a surplus of power (i.e. $P_{el} > P_{demand} + P_{PCU-losses}$) then the battery will be charged by the FCPM subject to its operational constraints (treated in Section 10), $P_{battery-charge}$.
- If there is an imbalance between the operating points of the FCPM, the battery, the PCU, and the demand, then the surplus or deficit will be handled by importation or exportation from the grid. (Grid-independent operation can be simulated with this scheme by using an appropriate external controller: refer to the first point above.)

The above control logic implies that a matching between the operating voltages of the FCPM, battery, and PCU. It is assumed that any efficiencies resulting from voltage-adjusting equipment is accounted for in the battery and PCU models.

2.4 Transient response

SOFC's tend to have slow transient response characteristics due to their high operating temperatures, large thermal inertia, and the thermal stresses that can be induced by sudden temperature changes within the stack. Given this reality, it is important to consider the transient behaviour of the FCPM for the following:

- To accurately model system control behaviour.
- To determine whether the FCPM will be able to follow load transients.
- To determine how the battery will be charged and discharged in order to respond to load transients.

The transient behaviour of the stack (only one of the components represented in the FCPM control volume, as discussed in Section 2 and illustrated in Figure II-3) is highly complex and the methods used to manage this transient behaviour are likely to be considered proprietary by manufacturers. Consequently, the explicit treatment of thermal transients is not considered in this model. Rather, the model limits the FCPM's transient response in three ways, this to enable the model to consider the impact that these transients have on overall system performance. Firstly, the response during normal operation is characterized by an input parameter that limits the change in operating point from one simulation time-step to the next. It is specified in terms of the maximum allowable time derivative of the FCPM's electrical output, $(dP_{el}/dt)_{\max}$ (W/s). This parameter is applied as follows to constrain the transient response of the FCPM,

$$If \quad \frac{\left| P_{el}^{t+\Delta t} - P_{el}^{t} \right|}{\Delta t} > \left(\frac{dP_{el}}{dt} \right)_{\max} \tag{II-11}$$

$$then \quad P_{el}^{t+\Delta t} = P_{el}^{t} \pm \left(\frac{dP_{el}}{dt} \right)_{\max} \cdot \Delta t$$

Where P_{el}^{t} is the FCPM's electrical output at the previous time-step and $P_{el}^{t+\Delta t}$ is the output at the current time-step (i.e. the time-step whose solution is sought). Equation II-11 assumes that the FCPM's internal controller imposes this behaviour and that the performance of the FCPM (e.g. fuel consumption, exhaust gas temperature) at the time-steps t and $t + \Delta t$ can be determined through quasi steady-state solutions. The FCPM's transient response may differ depending on whether the power input is increasing or decreasing. Therefore, two values could be supplied for $(dP_{el}/dt)_{\max}$, one associated with the positive sign in equation II-11 and one associated with the negative sign.

A second set of inputs will be specified to characterize the start-up period during which the stack is heated to its operating temperature and then its voltage gradually reduced to its operating point. The variable $\delta t_{start-up}$ represents this entire time period (both the warming phase and the voltage-reduction phase) following which the FCPM is considered to have achieved its nominal operating state. It is assumed that the stack is either warmed through the combustion of fuel or through electric resistance heating (some products may use both modes of heating during different points in time over $\delta t_{start-up}$). The FCPM may produce some electricity during the voltage-reduction phase of $\delta t_{start-up}$.

The following variables are to be specified by the user to characterize the performance during the start-up period:

- $\delta t_{start-up}$ is the duration of the start-up period (seconds), both its warming phase and its voltage-reduction phase.
- $kmol_{fuel,start-up} = \int_{0}^{\delta t_{start-up}} \dot{N}_{fuel,start-up} dt$ is the consumption of fuel (kmol) during $\delta t_{start-up}$.

  Note that $kmol_{fuel,start-up}$ represents the fuel consumed both through combustion during the warming phase (if this is the mechanism used for heating) and in the fuel cell itself and the afterburner during the voltage reduction phase.
- $E_{heat+anc\_start-up} = \int_{0}^{\delta t_{start-up}} P_{heat+anc\_start-up} dt$ is the electrical energy (MJ) supplied to the FCPM during $\delta t_{start-up}$. This includes both the energy consumed by the heating element

(if present) and any ancillaries such as controls and fans that are powered by AC electricity that is supplied to the cogeneration device. Note that the term $P_{el,ancillaries-AC}$ from equation II-1 is not active during start-up period so all ancillaries that are not powered directly by the stack's DC output (refer to the therm $E_{el,start-up}$ below) are considered in the term $E_{heat+anc\_start-up}$.

- $E_{el,start-up} = \int_0^{\delta t_{start-up}} P_{el,start-up}\,dt$ is the net DC electrical energy production (MJ) from the FCPM during $\delta t_{start-up}$. If ancillaries such as controls and fans that are necessary to manage the start-up phase are directly powered by the stack's DC output, then their consumption is accounted for in this term.

The control of the warming and the voltage-reduction phases of the start-up period can be quite complex and vary from manufacturer to manufacturer. The fuel and electrical supply and electrical production will be tightly controlled to protect the integrity of the stack and can vary considerably throughout $\delta t_{start-up}$. Notwithstanding, for the purposes of this model it is assumed that the rates of fuel and electrical consumption and electrical production are constant during the start-up period, that is $\dot{N}_{fuel,start-up} = kmol_{fuel,start-up}/\delta t_{start-up}$, $P_{heat+anc\_start-up} = E_{heat+anc\_start-up}/\delta t_{start-up}$, and $P_{el,start-up} = E_{el,start-up}/\delta t_{start-up}$. This is clearly a modelling artifact whose use is justified (necessary) because significantly more data would be required from the user to predict the temporal distribution of $\dot{N}_{fuel,start-up}$, $P_{heat+anc\_start-up}$, and $P_{el,start-up}$ throughout $\delta t_{start-up}$ and such data are likely be considered proprietary by manufacturers and thus unavailable. Furthermore, given the complex nature of starting and stopping a SOFC and the potential impact this can have upon durability, undoubtedly SOFC-cogeneration devices will be controlled to minimize stop-start cycles and thus the impact that these cycles will have simulation results over the durations of interest to Annex 42 will be minimal.

A third set of inputs will be specified for the cool-down period, $\delta t_{cool-down}$. During this time it is assumed that the FCPM produces no electrical output and that it cannot be completely turned off or switched back into operation until $\delta t_{cool-down}$ time has elapsed. Fuel and/or electricity can be consumed during the cool-down period to monitor and control the cooling process to avoid excessive thermal stresses.

The following variables are to be specified by the user to characterize the performance during the cool-down period:

- $\delta t_{cool-down}$ is the duration of the cool-down period (seconds).

- $kmol_{fuel,cool-down} = \int_0^{\delta t_{cool-down}} \dot{N}_{fuel,cool-down}\, dt$ is the consumption of fuel (kmol) during $\delta t_{cool-down}$.
- $E_{heat+anc\_cool-down} = \int_0^{\delta t_{cool-down}} P_{heat+anc\_cool-down}\, dt$ is the electrical energy (MJ) supplied to the FCPM during $\delta t_{cool-down}$. This includes both the energy consumed by the heating element (if present) and any ancillaries such as controls and fans that are powered by AC electricity that is supplied to the cogeneration device. Note that the term $P_{el,ancillaries-AC}$ from equation II-1 is not active during cool-down period so all ancillaries are considered in the term $E_{heat+anc\_cool-down}$.

Similar to the start-up period, it is assumed that the rates of fuel and electrical consumption are constant during the cool-down period.

It is important to note the approach outlined above for treating transients will not predict the thermal stresses induced by transient operation nor the impact of these stresses upon service life. These types of analyses require mechanistic models that examine single or a few operating scenarios. However, the model will be useful to place limits upon the FCPM's transient response which will enable the study of this aspect of the device upon overall system behaviour and performance over the a long-term simulation.

As described in the foregoing, the user must supply nine input parameters to characterize the FCPM's transient behaviour, $(dP_{el}/dt)_{max-dec}$, $(dP_{el}/dt)_{max-inc}$, $\delta t_{start-up}$, $kmol_{fuel,start-up}$, $E_{heat+anc\_start-up}$, $E_{el,start-up}$, $\delta t_{cool-down}$, $kmol_{fuel,cool-down}$, and $E_{heat+anc\_cool-down}$. Although these data may prove to be difficult to establish, a number of possible sources of information can be used:

- Data supplied by manufacturers.
- Data from the open literature.
- From controlled experiments conducted within Annex 42 (Beausoleil-Morrison and Kelly 2004) or from anecdotal observations during laboratory and field work conducted by Annex 42 participants.
- Derived from the results of detailed mechanistic models that explicitly simulate the electrochemical, thermochemical, and heat transfer transient reactions within stacks.

2.5 Fuel supply

The composition of the fuel stream will be defined by the user in terms of molar fractions, χ_i. This composition will be treated as static throughout the period of the simulation. The possible fuel constituents will be:

- Hydrogen (H_2).
- The hydrocarbons methane (CH_4), ethane (C_2H_6), propane (C_3H_8), butane (C_4H_{10}), pentane (C_5H_{12}), and hexane (C_6H_{14})[1].
- The alcohols methanol (CH_3OH) and ethanol (C_2H_5OH).
- The inert constituents carbon dioxide (CO_2) and nitrogen (N_2).
- Oxygen (O_2).

These constituents will allow the user to simulate a fuel cell supplied with virtually any natural gas mixture, propane, pure hydrogen, ethanol, or methanol.

Although sulphur odourants (e.g. mercaptons) are typically added to natural gas mixtures for safety reasons (leak detection), these do not appear in the list above because their molar fractions are very low (<0.001%). Additionally, these compounds will be removed by the desulphurizer located within the FCPM control volume.

Water vapour can also be found in natural gas mixtures. However, as the molar fraction of water is typically very low (<0.01%) it has been neglected from the above list.

The $\sum_i (\dot{N}_i \cdot [\hat{h}_i - \Delta_f \hat{h}_i^o])_{fuel}$ term of the energy balance represented by equation II-7 is evaluated using the Shomate equation (NIST 2003), which expresses the difference between a gas' enthalpy and its standard enthalpy of formation as a polynomial function of temperature,

$$\hat{h}_i - \Delta_f \hat{h}_i^o = A \cdot \left(\frac{T}{1\,000}\right) + \frac{B}{2} \cdot \left(\frac{T}{1\,000}\right)^2 + \frac{C}{3} \cdot \left(\frac{T}{1\,000}\right)^3 + \frac{D}{4} \cdot \left(\frac{T}{1\,000}\right)^4 - \frac{E}{\left(\frac{T}{1\,000}\right)} + F - H \qquad \text{(II-12)}$$

Where T is the temperature of gas i (K).

It is worth noting that the enthalpy ($\hat{h}_i$) of a gas can also be determined with equation II-12 since $\Delta_f \hat{h}_i^o$ is equal to H (the last term on the right side of the equation).

[1] Butane through hexane are typically found only in trace quantities (< 0.5%) in natural gas supplies. Consequently, the molar fractions of these constituents might be set to zero by the user with little sacrifice in accuracy.

For the purposes of evaluating the enthalpies of the fuel constituents, it is assumed that the fuel enters the FCPM control volume at the temperature of the exit of the fuel compressor control volume (state point 5 in Figure II-2; refer to Section 4).

The American National Institute of Standards and Technology provides the coefficients (A, B, C, D, E, F, and H) of the Shomate equation in its widely used Chemistry Webbook (NIST 2003). The NIST Chemistry Webbook coefficients for the following gases are used in this model: N_2, O_2, Ar, CO_2, H_2, and CH_4. These coefficients can be found in Appendix A of this document. The NIST Chemistry Webbook, however, does not include data for the higher hydrocarbons nor for the alcohol fuels. Additionally, its correlation for water vapour does not span the temperature range of interest for this model. Consequently, an alternate approach was used for these other gases. The correlation and coefficients proposed by Gordon and McBride (1971) were evaluated over a wide range of temperatures and then these data regressed to the form of equation II-12 to produce the A, B, C, D, E, F, and H coefficients. These coefficients can also be found in Appendix A.

The LHV of the fuel mixture is determined using the user-specified molar fractions,

$$LHV_{fuel} = \sum_i (\chi_i \cdot LHV_i) \tag{II-13}$$

Data from the NIST Chemistry Webbook are used to establish the LHV of each fuel constituent by recognizing that,

$$LHV_i = [\Delta_f \hat{h}^o_{C_x H_y} - x \cdot \Delta_f \hat{h}^o_{CO_2} - \tfrac{y}{2} \cdot \Delta_f \hat{h}^o_{H_2O}] \tag{II-14}$$

The standard enthalpies of formation for CO_2, H_2O, and each relevant fuel constituent will be compiled and provided in an appendix of a future version of this specification.

At each time-step of the simulation the net power output, P_{el}, is established using the methods elaborated in subsections 2.3 and 2.4. The electrical efficiency, ε_{el}, is subsequently determined using the approach described in subsection 2.2. Using these quantities, equation II-10 is solved to determine the total molar flow rate of all fuel constituents, $\dot{N}_{fuel}$ at that time-step. This total molar flow rate is then used in conjunction with the user-specified molar fractions and equation II-12 to establish the $\sum_i (\dot{N}_i \cdot [\hat{h}_i - \Delta_f \hat{h}^o_i])_{fuel}$ term in the energy balance represented by equation II-7.

2.6 Air supply

The composition of the air stream will be defined by the user in terms of molar fractions, χ_i. The air composition will be treated as static throughout the period of the simulation. The possible air

constituents will be N_2, O_2, H_2O, Ar, and CO_2. The user could choose to either specify molar fractions for all these constituents or may decide that it is sufficient to approximate air's composition by considering only the two major constituents, N_2 and O_2.

Three alternate methods are provided for establishing the flow rate of air introduced to the FCPM control volume.

Method 1

With the first method, the user specifies a constant excess air ratio (λ). The air flow rate is defined to be $(1+\lambda)$ times the stoichiometric air flow requirement. The stoichiometric oxygen requirement is determined based upon the stoichiometric reactions of the fuel constituents,

$$C_x H_y O_z + \left(x + \frac{y}{4} - \frac{z}{2}\right) \cdot O_2 \rightarrow x \cdot CO_2 + \frac{y}{2} \cdot H_2O \qquad \text{(II-15)}$$

Equation II-15 is applied to each of the fuel constituents to determine the stoichiometric oxygen requirement. These results are combined with the flow rates of the fuel constituents (refer to subsection 2.5), the user-specified excess air ratio, and the user-specified molar fractions for the composition of air to lead to the solution of the air flow rate for the time-step, $\dot{N}_{air}$.

Method 2

The first method for calculating the flow rate of air introduced to the FCPM control volume implies that the supply fan flow characteristics, supply ductwork, and fan control strategies are such that a constant ratio of air to fuel can be maintained. This assumption is dropped with the second method, which use a parametric relation to express the air flow as a function of the net electrical power output and the ambient air temperature,

$$\dot{N}_{air} = \left[a_0 + a_1 \cdot P_{el} + a_2 \cdot P_{el}^2\right] \cdot \left[1 + a_3 \cdot T_{air}\right] \qquad \text{(II-16)}$$

Where $\dot{N}_{air}$ is the molar flow rate of air (kmol/s) and T_{air} is the temperature of the air (°C) supplied to the FCPM. The a_i coefficients are supplied by the user. Empirical data, information from manufacturers, or analytic models can be used to establish these coefficients.

The $[1 + a_3 \cdot T_a]$ term in equation II-16 can be used to account for systems that cool the fuel cell stack using ambient air and thus adjust $\dot{N}_{air}$ in response to ambient conditions. It is assumed that the air enters the FCPM control volume (T_{air}) at the temperature of the exit of the air supply blower (state point 4 in Figure II-2; refer to Section 3).

Method 3

The third method is identical to the second, except that the air flow is given as a function of the fuel flow rate,

$$\dot{N}_{air} = \left[a_0 + a_1 \cdot \dot{N}_{fuel} + a_2 \cdot \dot{N}_{fuel}^2 \right] \cdot \left[1 + a_3 \cdot T_{air} \right] \qquad \text{(II-17)}$$

Again, the a_i coefficients are supplied by the user. These can be derived from empirical data, information from manufacturers, or analytic models.

At each time-step, the solution of $\dot{N}_{air}$ is used in conjunction with the user-specified molar fractions and the Shomate equation (equation II-12) to calculate the $\sum_i (\dot{N}_i \cdot [\hat{h}_i - \Delta_f \hat{h}_i^o])_{air}$ term of the energy balance represented by equation II-7. The enthalpies of the air constituents are evaluated at T_{air}.

2.7 Water supply

The model has been structured to give the user the option of specifying a liquid water input stream for steam reformation. In the case of internally reforming SOFCs that do not require water for steam reformation, the inlet water flow rate can be neglected.

The user will specify parametric coefficients that give the liquid water flow rate as a function of the fuel flow rate,

$$\dot{N}_{liq-water} = w_0 + w_1 \cdot \dot{N}_{fuel} + w_2 \cdot \dot{N}_{fuel}^2 \qquad \text{(II-18)}$$

Where $\dot{N}_{liq-water}$ is the molar flow rate of liquid water (kmol/s). The w_i coefficients can be established using empirical data, information from manufacturers, or analytic models.

Equation II-12 is used to calculate the $[\hat{h} - \Delta_f \hat{h}^o]_{H_2O,liq}$ term of the energy balance represented by equation II-7. For the purposes of evaluating the enthalpy of the water it is assumed that the water enters the FCPM control volume at the temperature of the exit of the water pump (state point 6 in Figure II-2; refer to Section 5).

By recognizing that $\Delta_f \hat{h}^o$ equals H in the Shomate equation, and that $\Delta_f \hat{h}^o_{H_2O,fg}$ is the difference between the standard enthalpies of formation of water vapour and liquid water (refer to equation II-6a), it can be seen that equation II-12 can also be used to establish the latent heat of vapourization of water at the standard state for equation II-7.

2.8 Product gases

The product gases exiting the FCPM control volume result from the the electrochemical and combustion reaction of the fuel and air that enter the control volume as well as the water vapour that is generated as a result of the introduction of liquid water for steam reformation purposes. This is represented by the $\sum_i (\dot{N}_i \cdot [\hat{h}_i - \Delta_f \hat{h}_i^o])_{FCPM-cg}$ terms in equation II-7.

Given the operating temperatures of the reformer, stack, and afterburner, it is expected that the emissions of hydrocarbons, hydrogen, CO, and NO_x from residential FC-cogeneration devices will be extremely low. Based upon the data presented by Karakoussis et al (2000), for example, it is expected that hydrocarbons and NO_x emissions will represent about 0.2% of the exhaust, a level similar to that found with automotive engines. And the level of CO and SO_x emissions is expected to much lower than this, two orders of magnitude lower than automotive engines.

These emissions levels are insignificant in terms of the energy balance on the FCPM control volume. Therefore, for the purposes of establishing the $\sum_i (\dot{N}_i \cdot [\hat{h}_i - \Delta_f \hat{h}_i^o])_{FCPM-cg}$ term in equation II-7 the hydrogen, hydrocarbons, and alcohols supplied to the FCPM can be assumed to fully react to CO_2 and H_2O, as given in equation II-15.

At each time-step, once the flow rates of the fuel and air constituents are established, the flow rate of each product constituent resulting from electrochemical and combustion reactions can be determined using equation II-15. It is assumed that the inert fuel and air constituents (Ar and N_2) and the excess O_2 pass through the control volume unreacted.

When liquid water that has been supplied for steam reformation purposes (refer to subsection 2.7) it can be considered to react with methane as described in the following overall reaction,

$$CH_4 + 2H_2O \rightarrow 4H_2 + CO_2 \qquad \text{(II-18a)}$$

The H_2 produced by steam reformation is reacted in the fuel cell and afterburner according to the overall reaction given in equation II-15. The CO_2 produced by steam reformation is equal to the quantity that would be produced by the direct internal reforming of CH_4 in the fuel cell. Examination of equations II-15 and II-18a reveals that the quantity of water introduced for steam reformation will increase the water vapour content of the FCPM product gases by the same amount.

Therefore, the impact of steam reformation on the composition of the product gas stream can be determined by adding the flow rate of water determined with equation II-18 to the product gases as determined in the above paragraph. Having established the composition of the product gas stream, the Shomate equation (equation II-12) is used to establish the $\sum_i (\dot{N}_i \cdot [\hat{h}_i - \Delta_f \hat{h}_i^o])_{FCPM-cg}$ term in equation II-7. This is state point 7 in Figure II-2.

2.9 Ancillaries included in FCPM that are powered by AC

The $P_{el,ancillaries-AC}$ term in equation II-7 represents the power draw of the ancillaries that are included within the control volume and that are powered by AC electricity that is supplied to the cogeneration device.

A first-order expression is used to evaluate this term,

$$P_{el,ancillaries-AC} = anc_0 + anc_1 \cdot \dot{N}_{fuel} \tag{II-19}$$

Where $\dot{N}_{fuel}$ is the molar flow rate of the fuel mixture and is given by $\dot{N}_{fuel} = \sum_i (\chi \dot{N})_i$ where χ_i is the molar fraction of fuel constituent *i* (refer to subsection 2.5).

This formulation assumes that the ancillary power draws are proportional to the fuel supply rate with anc_0 representing the stand-by consumption.

2.10 Skin losses

$q_{skin-loss}$ in equation II-7, which represents the parasitic thermal losses from the FCPM control volume to the containing room via radiation and convection, is perhaps the most difficult term to accurately quantify. It is hoped that the experimental work conducted within Annex 42 will accurately characterize this term.

It is important to note that some FC-cogeneration devices may recover the thermal energy from the FCPM by drawing the supply air through the cabinet containing the FCPM. This is shown schematically in Figure II-3 with a short dashed line. Since this process occurs within the control volume it is not represented by the energy balance of equation II-7. Rather, $q_{skin-loss}$ is defined to represent only the portion of the heat loss from the FCPM that is transferred to the containing room.

Three alternate methods provide the user flexibility in modelling the $q_{skin-loss}$ term.

Method 1

With the first method the user simply specifies a constant value for $q_{skin-loss}$ (W). It is assumed that the losses are equal to this value during all time-steps in which the fuel cell is operating.

Method 2

With the second method it is assumed that the losses are proportional to the temperature difference between the product gases and the air in the room containing the FC-cogeneration device,

$$q_{skin-loss} = (UA) \cdot (T_{FCPM-cg} - T_{room}) \tag{II-20}$$

Where (*UA*) a heat loss coefficient supplied by the user (W/K) that characterizes the convection and radiation from the skin of the FCPM control volume to the containing room. T_{room} is the air temperature of the room (e.g. basement, garage) that contains the FC-cogeneration device. It is important to note that (*UA*) is not a function of the temperature difference between the surface of the FCPM and the room air nor a function of the temperature difference between the external surface of the FC-cogeneration device and the room air, but rather between the FCPM product gases and the room air. This is necessary as the placement of the control volume that represents the FCPM precludes the explicit solution of surface temperatures. $T_{FCPM-cg}$ was selected as an appropriate reference temperature for the skin losses since there should be a correlation between it and the surface temperatures.

Method 3

With the third method $q_{skin-loss}$ is expressed as a function of the fuel flow rate,

$$q_{skin-loss} = s_0 + s_1 \cdot \dot{N}_{fuel} + s_2 \cdot \dot{N}_{fuel}^2 \qquad \text{(II-21)}$$

Empirical data (perhaps from the Annex 42 experimental work), information from manufacturers, or analytic models can be used to establish the (*UA*) term for equation II-20 or the s_i coefficients for equation II-21.

Regardless of which method is employed, $q_{skin-loss}$ will be added as a source term to the energy balance representing the room that contains the FC-cogeneration device. The user will specify the convective/radiative split of $q_{skin-loss}$. This split will be invariant over the simulation.

2.11 Dilution air

For cooling purposes, some FC-cogeneration devices may draw air from the containing room, through the cabinet containing the FCPM, and subsequently add it to the dilution air/HRV control volume. This is to be distinguished from designs wherein the air drawn from the room is subsequently supplied to the FCPM (refer to subsection 2.10).

The user specifies the flow rate of the dilution air that is drawn in at the containing room's air temperature (state point 20 in Figure II-2). The composition of this air is determined based upon the inputs given for the supply air stream (refer to subsection 2.6). This information fully defines the $\dot{H}_{dilution-air-in}$ term in equation II-7. The $\dot{H}_{dilution-air-out}$ term in equation II-7 is determined as detailed in Section 9.

In modelling an FC-cogeneration device in which this design feature is not used, these terms can be easily nullified in the energy balance of equation II-7 by setting the dilution air flow rate to zero.

3. Air Supply Blower

Some building simulation programs may already contain component models for fans that could be used to represent the air supply blower using the techniques outlined here.

The following energy balance can be written for the blower's control volume,

$$\dot{H}_{blower-in} + P_{blower,el} + q_{aux-skin-loss} + q_{battery-loss} + q_{PCU-loss} + q_{air-cooler} \qquad \text{(II-22)}$$

$$= \dot{H}_{blower-out} + q_{blower-heat-loss}$$

Where $\dot{H}_{blower-in}$ and $\dot{H}_{blower-out}$ are the flow rates of the enthalpy (W) of the air entering (state point 1 in Figure II-2) and exiting (state point 4 in Figure II-2) the blower. $P_{blower,el}$ is the AC electrical power consumption of the blower's motor (W). And $q_{blower-heat-loss}$ is the heat loss from the blower, that is the heat output from the motor and fan that is not added to the air stream (W). It is assumed that this heat loss is added to the energy balance representing the room containing the FC-cogen device.

As shown schematically in Figure II-1, heat can be recovered from the battery, PCU, auxiliary burner and the stack cooling system for the purposes of pre-heating in the FCPM's air intake. This could be accomplished by using an airtight enclosure and by drawing air from within the enclosure. In this case the user may specify that the heat loss from these control volumes is added to the air stream before it enters the FCPM. $q_{aux-skin-loss}$ in equation II-22 represents the heat loss from the auxiliary burner that is recovered for pre-heating the air intake (refer to Section 6). $q_{battery-loss}$, $q_{PCU-loss}$ and $q_{air-cooler}$ represent similar terms for the battery, PCU and the air-cooler that rejects heat from the stack cooling system (refer to Sections10, 11 and 8).

Since there are no chemical reactions between the inlet and outlet streams and the temperature rise is moderate, the enthalpies can be expressed with the air's temperature rise and a heat capacity,

$$\dot{H}_{blower-out} - \dot{H}_{blower-in} = \dot{N}_{air} \cdot \hat{c}_P \cdot (T_{blower-out} - T_{blower-in}) \qquad \text{(II-23)}$$

Where $\dot{N}_{air}$ is the air flow rate (kmol/s) and is assumed to be same air flow rate that enters the FCPM control volume (i.e. there is no leakage in the ducting system). $\hat{c}_P$ is the heat capacity (J/kmolK) of the air evaluated at the inlet temperature to the blower, $T_{blower-in}$ (°C). And $T_{blower-out}$ is the temperature of the air that is delivered by the blower to the FCPM control volume (°C).

The user is given two choices for establishing $T_{blower-in}$. The air can either be drawn from the room that contains the FC-cogeneration device or from the outdoors. In the former case this can be considered as an unbalanced mechanical exhaust from the room and its impact upon the

room's air infiltration rate should be considered in the energy balance of the containing room.

$P_{blower,el}$ is expressed as a function of the air flow rate through the blower,

$$P_{blower-el} = b_0 + b_1 \cdot \dot{N}_{air} + b_2 \cdot \dot{N}_{air}^2 + b_3 \cdot \dot{N}_{air}^3 \quad \text{(II-24)}$$

The b_i coefficients are supplied by the user. Empirical data, information from manufacturers, or analytic models can be used to establish these coefficients.

The heat loss from the blower is a function of the placement of the motor and the thermal insulation of the blower and the ductwork included within the control volume. This is characterized by the user in terms of a fraction of the electrical input to the blower,

$$\alpha_{blower-heat-loss} = \frac{q_{blower-heat-loss}}{P_{blower-el}} \quad \text{(II-25)}$$

The user can make use of empirical data, information from manufacturers, or analytic models to establish $\alpha_{blower-heat-loss}$.

Combining equations II-23 and II-25 into equation II-22 leads to the following form of the energy balance, where $P_{blower-el}$ is established with equation II-24,

$$\dot{N}_{air} \cdot \hat{c}_P \cdot (T_{blower-out} - T_{blower-in}) = (1 - \alpha_{blower-heat-loss}) \cdot P_{blower-el} \quad \text{(II-26)}$$

$$+ q_{aux-skin-loss} + q_{battery-loss} + q_{PCU-loss} + q_{air-cooler}$$

This modelling approach allows flexibility in the treatment of the air supply blower. The user may have access to empirical data that aggregates the performance of the blower with that of the FCPM, i.e. the blower is included in $P_{el,ancillaries-DC}$ in equation II-9 or in $P_{el,ancillaries-AC}$ in equation II-7. In this case, the user can set $\alpha_{blower-heat-loss}$ and the b_i coefficients to zero. This effectively includes the blower within the FCPM control volume while nullifying the blower control volume.

4. Fuel Supply Compressor

Some building simulation programs may already contain component models for compressors that could be used to represent the fuel supply compressor using the techniques described here.

An energy balance can be written for the compressor similar to the one formed for the air supply blower (refer to Section 3),

$$\dot{N}_{fuel} \cdot \hat{c}_P \cdot (T_{comp-out} - T_{comp-in}) = (1 - \alpha_{comp-heat-loss}) \cdot P_{comp-el} \quad \text{(II-27)}$$

Where $\dot{N}_{fuel}$ and $\hat{c}_P$ are the flow rate (kmol/s) and heat capacity (J/kmolK) of the fuel. $T_{comp-in}$ and $T_{comp-out}$ and the temperatures of the fuel flowing into (state point 2 in Figure II-2) and out of (state point 5 in Figure II-2) the compressor control volume (°C).

The user is given two choices for establishing $T_{comp-in}$. The fuel can either be drawn from the room that contains the FC-cogeneration device or from the outdoors.

The AC electrical power consumption of the compressor, $P_{comp,el}$ (W), is expressed as a function of the fuel flow rate through the compressor,

$$P_{comp-el} = c_0 + c_1 \cdot \dot{N}_{fuel} + c_2 \cdot \dot{N}_{fuel}^2 + c_3 \cdot \dot{N}_{fuel}^3 \quad \text{(II-28)}$$

$\alpha_{comp-heat-loss}$ in equation II-27 represents the ratio of the heat loss from the compressor to the electrical input to the compressor. It is assumed that this heat loss is added to the energy balance representing the room containing the FC-cogen device.

This modelling approach allows flexibility in the treatment of the fuel compressor. The user may have access to empirical data that aggregates the performance of the compressor with that of the FCPM, i.e. the compressor is included in $P_{el,ancillaries-DC}$ in equation II-9 or in $P_{el,ancillaries-AC}$ in equation II-7. In this case, the user can set $\alpha_{comp-heat-loss}$ and the c_i coefficients to zero. This effectively includes the fuel compressor within the FCPM control volume while nullifying the compressor control volume. Similarly, if the FC-cogeneration device does not include a fuel compressor (i.e. the pressure of the gas supplied to the building is sufficient) the user simply sets $\alpha_{comp-heat-loss}$ and the c_i coefficients to zero.

5. Water Pump

Some building simulation programs may already contain component models for pumps that could be used to represent the water supply pump using the techniques described here.

An energy balance can be written for the pump similar to the one formed for the air supply blower (refer to Section 3),

$$\dot{N}_{liq-water} \cdot \hat{c}_P \cdot (T_{pump-out} - T_{pump-in}) = (1 - \alpha_{pump-heat-loss}) \cdot P_{pump-el} \qquad \text{(II-29)}$$

Where $\dot{N}_{liq-water}$ and $\hat{c}_P$ are the flow rate (kmol/s) and heat capacity (J/kmolK) of the water. $T_{pump-in}$ and $T_{pump-out}$ and the temperatures of the water flowing into (state point 3 in Figure II-2) and out of the pump control volume (°C). (state point 6 in Figure II-2)

The user is given two choices for establishing $T_{pump-in}$. The water can either be drawn from the room that contains the FC-cogeneration device or from the water mains.

The AC electrical power consumption of the pump, $P_{pump-el}$ (W), is expressed as a function of the water flow rate through the pump,

$$P_{pump-el} = p_0 + p_1 \cdot \dot{N}_{water} + p_2 \cdot \dot{N}_{water}^2 + p_3 \cdot \dot{N}_{water}^3 \qquad \text{(II-30)}$$

$\alpha_{pump-heat-loss}$ in equation II-29 represents the ratio of the heat loss from the pump to the electrical input to the pump. It is assumed that this heat loss is added to the energy balance representing the room containing the FC-cogen device.

This modelling approach allows flexibility in the treatment of the water pump. The user may have access to empirical data that aggregates the performance of the pump with that of the FCPM, i.e. the pump is included in $P_{el,ancillaries-DC}$ in equation II-9 or in $P_{el,ancillaries-AC}$ in equation II-7. In this case, the user can set $\alpha_{pump-heat-loss}$ and the p_i coefficients to zero. This effectively includes the water pump within the FCPM control volume while nullifying the pump control volume. Similarly, if the FC-cogeneration device does not include a pump the user simply sets $\alpha_{pump-heat-loss}$ and the p_i coefficients to zero.

6. Auxiliary Burner

Some FC-cogeneration devices may contain an integrated auxiliary burner for providing back-up heating. The Sulzer-Hexis system, for example, contains an integrated auxiliary burner and a double-chamber heat exchanger (Diethelm 2004). The combustion gases from the FCPM are directed through one chamber of the heat exchanger and the exhaust gases from the auxiliary burner through the second chamber. The building's plant circulates water through the heat exchanger to extract energy from both gas streams concurrently.

The auxiliary burner and heat exchanger are represented with separate control volumes. This section treats the auxiliary burner control volume whereas the heat exchanger control volume is the subject of Section 7.

Although some FC-cogeneration systems may be configured with double-chamber heat exchangers, this model treats the combustion gases from the FCPM and the exhaust gases from the auxiliary burner as a single stream. It is felt that this modelling artifact will accurately represent the heat transfer from the enthalpy flow of the two gas streams while providing the model with flexibility for resolving various design configurations. Additionally, the control volume representing the auxiliary burner can be nullified in the case of designs where the auxiliary heating is either not present or accomplished elsewhere in the plant system (e.g. a burner within a water storage tank).

A schematic representation of the auxiliary burner control volume is illustrated in Figure II-4. The control volume is represented by two sections to facilitate the description of its mathematical model: a burner section and a mixing section.

An energy balance can be written for the burner section as follows,

$$\dot{H}_{aux-fuel} + \dot{H}_{aux-air} + P_{el,aux-ancillaries} = \dot{H}_{aux-cg} + q_{aux-skin-loss} \qquad \text{(II-31)}$$

Where $\dot{H}_{aux-fuel}$ and $\dot{H}_{aux-air}$ are the total enthalpy flow rates (W) of the fuel (state point 8 in Figure II-2) and air (state point 9 in Figure II-2) that are supplied to the control volume. $\dot{H}_{aux-cg}$ is the total enthalpy flow rate of the burner's combustion gases which exit the burner section and enter the mixing section (state point 10 in Figure II-2)

The flow rate of air introduced to the burner section (necessary for evaluating $\dot{H}_{aux-air}$) is determined from the stoichiometric oxygen requirement (refer to equation II-15) and from a constant user-specified excess air ratio. The user can specify whether this air is drawn at the temperature of the room that contains the FC-cogeneration device or at the outdoor air temperature. Similarly, the user can specify whether the fuel is supplied at room or outdoor air temperature. It is assumed that the fuel mixture supplied to the auxiliary burner is the same as that supplied to the FCPM (refer to subsection 2.5).

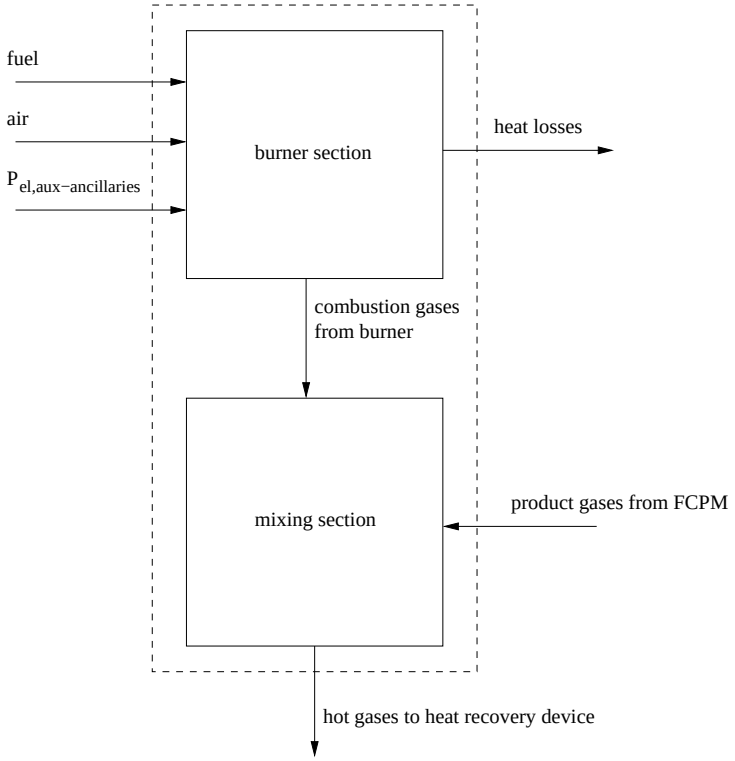

Figure II-4: Schematic of auxiliary burner control volume

$P_{el,aux-ancillaries}$ in equation II-31 is the AC electrical power (W) supplied to the auxiliary burner's ancillary devices (e.g. combustion air supply fan, controls, ignition system). It is assumed that all of the electrical power supplied to these ancillaries is added to the control volume. A first-order expression is used to evaluate this term,

$$P_{el,aux-ancillaries} = x_0 + x_1 \cdot \dot{N}_{aux-fuel} \tag{II-32}$$

Where $\dot{N}_{aux-fuel}$ is the molar flow rate of the fuel mixture combusted in the auxiliary burner and is given by $\dot{N}_{aux-fuel} = \sum_i (\chi \dot{N})_i$ where χ_i is the molar fraction of fuel constituent i (refer to subsection 2.5).

This formulation assumes that the ancillary power draws of the auxiliary burner are proportional to the burner's fuel supply rate. When the burner is inoperative then $P_{el,aux-anc}$ will be zero (refer to discussion below regarding the user-specified minimum burner output).

$q_{aux-skin-loss}$ in equation II-31 is the heat loss (W) from the burner, that is the portion of the energy from the combustion of the fuel that does not leave the burner section in the gas stream (i.e. $\dot{H}_{aux-cg}$). As shown in Figure II-1 and discussed in Section 3, $q_{aux-skin-loss}$ can either be lost to the containing room or can be recovered to heat the FCPM's air intake. It is assumed that this

heat transfer is proportional to the temperature difference between the gases exiting the auxiliary burner control volume and the air in the room containing the FC-cogeneration device,

$$q_{aux-skin-loss} = (UA)_{aux} \cdot (T_{aux\text{-}mix} - T_{room}) \tag{II-33}$$

Where $(UA)_{aux}$ a heat loss coefficient supplied by the user (W/K) that characterizes the convection and radiation from the skin of the auxiliary burner to the containing room. T_{room} is the air temperature of the room (e.g. basement, garage) that contains the FC-cogeneration device. It is important to note that $(UA)_{aux}$ is not a function of the temperature difference between the surface of the auxiliary burner and the room air, but rather between the gases exiting the control volume and the room air. This is necessary as the placement of the control volume that represents the auxiliary burner precludes the explicit solution of the surface temperature. $T_{aux\text{-}mix}$ was selected as an appropriate reference temperature for the skin losses since there should be a correlation between it and the surface temperature. When the burner is inoperative then $q_{aux-skin-loss}$ will be zero.

By assuming that the combustion of the fuel is complete, the LHV of the fuel can be introduced into the energy balance, as was done in subsection 2.1. With this, equation II-31 can be represented by,

$$\sum_i (\dot{N}_i \cdot [\hat{h}_i - \Delta_f \hat{h}_i^o])_{aux-fuel} + \sum_i (\dot{N}_i \cdot [\hat{h}_i - \Delta_f \hat{h}_i^o])_{aux-air} + P_{el,aux-ancillaries} \tag{II-34}$$

$$+ \dot{N}_{aux-fuel} \cdot LHV_{aux-fuel} = \sum_i (\dot{N}_i \cdot [\hat{h}_i - \Delta_f \hat{h}_i^o])_{aux\text{-}cg} + q_{aux-skin-loss}$$

As the combustion gases leave the burner section at high temperature, its H_2O will be in vapour form. Hence, the fuel's LHV, and not its HHV, appear in equation II-34.

The enthalpy terms of equation II-34, $\sum_i (\dot{N}_i \cdot [\hat{h}_i - \Delta_f \hat{h}_i^o])_{aux-fuel}$, $\sum_i (\dot{N}_i \cdot [\hat{h}_i - \Delta_f \hat{h}_i^o])_{aux-air}$, and $\sum_i (\dot{N}_i \cdot [\hat{h}_i - \Delta_f \hat{h}_i^o])_{aux\text{-}cg}$ are evaluated using the methods elaborated in subsections 2.5, 2.6, and 2.8. And $LHV_{aux-fuel}$ is determined using the method described in subsection 2.5.

The burner's capacity, expressed either in heat output (W) or fuel input (kmol/s), is specified by the user. It is assumed that the burner can fully modulate from a minimum (user-specified) output to full capacity and that its operating point is controlled by a signal originating elsewhere in the plant system, e.g. a water storage tank temperature or the temperature of water returned from space-heating radiators.

Referring to Figure II-4 and assuming that the mixing section is adiabatic, molar and energy balances can be written for the mixing section as follows,

$$\dot{N}_{aux-cg,i} + \dot{N}_{FCPM-cg,i} = \dot{N}_{aux-mix,i} \tag{II-35}$$

$$\sum_i (\dot{N}_i \cdot [\hat{h}_i - \Delta_f \hat{h}_i^o])_{aux\text{-}cg} + \sum_i (\dot{N}_i \cdot [\hat{h}_i - \Delta_f \hat{h}_i^o])_{FCPM-cg} = \sum_i (\dot{N}_i \cdot [\hat{h}_i - \Delta_f \hat{h}_i^o])_{aux\text{-}mix} \tag{II-36}$$

Where equation II-35 applies for each constituent gas (i), e.g. CO_2, H_2O, N_2.

The term $\sum_i (\dot{N}_i \cdot [\hat{h}_i - \Delta_f \hat{h}_i^o])_{FCPM-cg}$ is the enthalpy flow rate relative to the standard state (W) of the gases exiting the FCPM control volume and entering the auxiliary burner control volume (state point 7 in Figure II-2; refer to equation II-7). $\sum_i (\dot{N}_i \cdot [\hat{h}_i - \Delta_f \hat{h}_i^o])_{aux\text{-}mix}$ represents the enthalpy flow rate relative to the standard state (W) of the gases exiting the auxiliary burner control volume and entering the gas-side of the heat recovery device (state point 11 in Figure II-2).

As previously stated, the auxiliary heater control volume can be easily nullified in the case of modelling FC-cogeneration systems where the auxiliary heating is either not present or accomplished elsewhere in the plant system. In this case equations II-31 through II-36 will reduce to a form that represents a flow-through control volume in which the flow rate and enthalpy of the gases exiting equal to the entering values.

7. Exhaust-Gas-to-Water Heat Exchanger

Some building simulation programs may already contain component models that could be used to represent the gas-to-water heat exchanger using the techniques described here.

Four alternate methods are given for characterizing the device that transfers heat from the auxiliary burner (or FCPM) control volume exhaust gases to the water loop connected to the building's plant (i.e. the FC-cogeneration device's thermal output).

Method 1

With the first method the user provides a fixed heat exchanger effectiveness (ε_{HX}). At each time-step of the simulation this is used to calculate the heat recovery based upon the approach temperature, the difference between the temperature of the gases that exit the auxiliary burner control volume (or the FCPM control volume if the auxiliary burner is not present) and that enter the heat exchanger ($T_{aux\text{-}mix}$; state point 11 in Figure II-2) and the temperature of the water supplied to the heat exchanger by the plant ($T_{water,in}$; state point 12 in Figure II-2),

$$q_{HX} = \varepsilon_{HX} \cdot (\dot{N}\hat{c}_P)_{\min} \cdot (T_{aux\text{-}mix} - T_{water,in}) \tag{II-37}$$

Where $(\dot{N}\hat{c}_P)_{\min}$ is the minimum value of $(\dot{N}\hat{c}_P)_{aux\text{-}mix}$ and $(\dot{N}\hat{c}_P)_{water}$ for the current time-step.

The Schomate equation (NIST 2003) is used to determine the molar heat capacity of the gas stream as a polynomial function of temperature,

$$\hat{c}_{P,i} = A + B \cdot \left(\frac{T}{1\,000}\right) + C \cdot \left(\frac{T}{1\,000}\right)^2 + D \cdot \left(\frac{T}{1\,000}\right)^3 + \frac{E}{\left(\frac{T}{1\,000}\right)^2} \tag{II-38}$$

Where T is the temperature of gas constituent i. Equation II-38 is evaluated for each constituent of the gas stream entering the heat exchanger and the molar heat capacity of the gas mixture is determined by a weighted sum,

$$\hat{c}_P = \sum_i (\chi_i \cdot \hat{c}_{P,i}) \tag{II-39}$$

Where χ_i are the molar fractions of the gases entering the heat exchanger.

This first method can be useful in the analysis of hypothetical systems where the performance characteristics of the heat transfer device are unknown.

Method 2

The second and third methods employ the log mean temperature difference (LMTD) method to determine the heat recovery,

$$q_{HX} = (UA)_{eff} \cdot \frac{(T_{aux\text{-}mix} - T_{water,out}) - (T_{HX\text{-}exh} - T_{water,in})}{\ln\left(\frac{T_{aux\text{-}mix} - T_{water,out}}{T_{HX\text{-}exh} - T_{water,in}}\right)} \quad \text{(II-40)}$$

Where $T_{HX\text{-}exh}$ is the temperature of the cooled gases that are exhausted from the heat exchanger and that enter the optional air dilution system/HRV (state point 14 in Figure II-2) and $T_{water,out}$ is the temperature of the warmed water exiting the heat exchanger (state point 13 in Figure II-2).

If it is assumed that heat loss from the heat exchanger to the ambient is negligible and that the heat capacity of each fluid stream remains constant through the heat exchanger, then the following energy balance can be written for the heat transfer between the fluid streams,

$$q_{HX} = (\dot{N}\hat{c}_P)_{aux-mix} \cdot (T_{aux\text{-}mix} - T_{HX\text{-}exh}) = (\dot{N}\hat{c}_P)_{water} \cdot (T_{water,out} - T_{water,in}) \quad \text{(II-41)}$$

Where $\hat{c}_{P,aux-mix}$ is determined with equation II-39.

Equation II-41 can be rearranged to express the outlet water temperature as a function of the water inlet temperature and the gas temperatures,

$$T_{water,out} = T_{water,in} + \frac{(\dot{N}\hat{c}_P)_{aux-mix}}{(\dot{N}\hat{c}_P)_{water}} \cdot (T_{aux\text{-}mix} - T_{HX\text{-}exh}) \quad \text{(II-42)}$$

By substituting equation II-42 into the numerator of equation II-40 and by replacing q_{HX} with $(\dot{N}\hat{c}_P)_{aux-mix} \cdot (T_{aux\text{-}mix} - T_{HX\text{-}exh})$, it can be shown that,

$$\ln\left(\frac{T_{aux\text{-}mix} - T_{water,out}}{T_{HX\text{-}exh} - T_{water,in}}\right) = \frac{(UA)_{eff}}{(\dot{N}\hat{c}_P)_{aux-mix}} \cdot \left[1 - \frac{(\dot{N}\hat{c}_P)_{aux-mix}}{(\dot{N}\hat{c}_P)_{water}}\right] \quad \text{(II-43)}$$

By taking the exponential of each side of equation II-43, substituting in equation II-42, and rearranging, the gas outlet temperature can be expressed as a function of gas and water inlet temperatures,

$$T_{HX\text{-}exh} = \left\{\frac{1 - \frac{(\dot{N}\hat{c}_P)_{aux-mix}}{(\dot{N}\hat{c}_P)_{water}}}{\exp\left[(UA)_{eff} \cdot \left(\frac{1}{(\dot{N}\hat{c}_P)_{aux-mix}} - \frac{1}{(\dot{N}\hat{c}_P)_{water}}\right)\right] - \frac{(\dot{N}\hat{c}_P)_{aux-mix}}{(\dot{N}\hat{c}_P)_{water}}}\right\} \cdot T_{aux\text{-}mix} \quad \text{(II-44)}$$

$$+\left\{\frac{\exp\left[(UA)_{eff}\cdot\left(\frac{1}{(\dot{N}\hat{c}_P)_{aux-mix}}-\frac{1}{(\dot{N}\hat{c}_P)_{water}}\right)\right]-1}{\exp\left[(UA)_{eff}\cdot\left(\frac{1}{(\dot{N}\hat{c}_P)_{aux-mix}}-\frac{1}{(\dot{N}\hat{c}_P)_{water}}\right)\right]-\frac{(\dot{N}\hat{c}_P)_{aux-mix}}{(\dot{N}\hat{c}_P)_{water}}}\right\}\cdot T_{water,in}$$

With the LMTD approach the effective heat transfer coefficient must be evaluated at each time-step of the simulation. This second method for characterizing the heat exchanger employs an empirical approach which casts $(UA)_{eff}$ as a parametric relation with the water and product gas flow rates,

$$(UA)_{eff} = hx_{s,0} + hx_{s,1}\cdot\dot{N}_{water} + hx_{s,2}\cdot\dot{N}^2_{water} + hx_{s,3}\cdot\dot{N}_{aux\text{-}mix} + hx_{s,4}\cdot\dot{N}^2_{aux\text{-}mix} \quad \text{(II-45)}$$

This method can be particularly useful when empirical data are available from the testing of a specific heat exchange device over a range of water inlet and product gas temperatures. Such experimental data can be easily regressed to provide the $hx_{s,i}$ coefficients. It is worth noting the empirical form of equation II-45 compensates for some of the assumptions inherent to the LMTD method, namely the assumptions that there is no heat loss from the heat exchanger and that the fluid heat capacities are constant throughout the heat exchanger.

Method 3

The third method also calculates the heat transfer using the LMTD method and utilizes the equation II-44 form of the energy balance. But in this case $(UA)_{eff}$ is cast in an idealized form based upon more fundamental heat transfer processes.

By assuming that the heat transfer from the heat exchanger to each fluid stream can be expressed with a heat transfer coefficient that considers the convective and radiative processes and by assuming that conduction through the solid heat exchanger is one-dimensional, the resistance to heat transfer from the gas stream to the water stream can be expressed as,

$$R = \frac{1}{(hA)_{gas}} + \frac{t}{(kA)_{solid}} + \frac{1}{(hA)_{water}} \quad \text{(II-46)}$$

Where $(hA)_{gas}$ and $(hA)_{water}$ are the products of the heat transfer coefficient and heat exchange area on the gas and water sides of the heat exchanger, respectively. t is the thickness of the solid portion of the heat exchanger, k_{solid} its conductivity, and A_{solid} the heat exchange area of the solid.

By neglecting the resistance offered by conduction through the solid and by introducing an adjustment factor to compensate for the errors inherent in the assumptions of equation II-46 (e.g.

that the wall temperatures of the heat exchanger are uniform) and those of the LMTD method, the effective heat transfer coefficient can be expressed as,

$$(UA)_{eff} = [R + F_{HX}]^{-1} \tag{II-47}$$

$$= \left[\frac{1}{(hA)_{gas}} + \frac{1}{(hA)_{water}} + F_{HX} \right]^{-1}$$

Where F_{HX} is the adjustment factor.

The heat transfer coefficients are treated as functions of the fluid flow rates as follows,

$$h_{gas} = h^0_{gas} \cdot \left(\frac{\dot{N}_{gas}}{\dot{N}^0_{gas}} \right)^n \tag{II-48}$$

$$h_{water} = h^0_{water} \cdot \left(\frac{\dot{N}_{water}}{\dot{N}^0_{water}} \right)^m$$

Where h^0_j is the heat transfer coefficient at the nominal flow rate $\dot{N}^0_j$. These empirical constants as well as the empirical constants *n* and *m* are supplied by the user. The user also supplies A_{gas}, A_{water}, and the empirical constant F_{HX}.

Maréchal (2004) indicates how these empirical constants can be identified from experimental results at a single operating point.

Method 4

The first three methods are appropriate when there is only sensible heat exchange from the gas stream to the heat exchanger whereas this fourth method is applicable for condensing heat exchangers.

The fourth method is based upon method 2 with an additional term is added to account for the augmentation in heat transfer due to condensation,

$$q_{HX} = q_{sensible} + q_{latent} \tag{II-49}$$

$$= (UA)_{eff} \cdot \frac{(T_{aux\text{-}mix} - T_{water,out}) - (T_{HX\text{-}exh} - T_{water,in})}{\ln\left(\frac{T_{aux\text{-}mix} - T_{water,out}}{T_{HX\text{-}exh} - T_{water,in}} \right)} + \dot{N}_{H_2O-cond} \cdot \hat{h}_{fg}$$

Where $\dot{N}_{H_2O-cond}$ is the rate of condensation of water from the gas stream (kmol/s) and $\hat{h}_{fg}$ is the

molar heat of vapourization of water (J/kmol).

The sensible component of the heat exchange is determined using an empirically derived $(UA)_{eff}$ coefficient (refer to equation II-45). Similarly, the rate of condensation is expressed in a parametric form that facilitates the determination of its coefficients from empirical data. The functional form of this parametric equation was established by recognizing that, for a given heat exchanger, the rate of condensation will be primarily influenced by the concentration of water vapour in the gas stream and by the difference between the heat exchanger's temperature and the gas's dew point,

$$\dot{N}_{H_2O-cond} = (T_{cond-threshold} - T_{water,in}) \cdot \left[hx_{l,1} \cdot \left(\frac{\dot{N}_{H_2O}}{\dot{N}_{aux-mix}} \right) + hx_{l,2} \cdot \left(\frac{\dot{N}_{H_2O}}{\dot{N}_{aux-mix}} \right)^2 \right] \quad \text{(II-50)}$$

$\dot{N}_{H_2O}$ in equation II-50 is the molar flow rate of water vapour in the gas stream entering the heat exchanger and $\dot{N}_{aux-mix}$ is the molar flow rate of all gases.

$T_{cond-threshold}$ is a user-specified fixed value that represents the threshold of the water-inlet temperature above which condensation will not occur. When $T_{water,in}$ is below $T_{cond-threshold}$ the condensation rate will be determined with equation II-50. And when $T_{water,in}$ is above $T_{cond-threshold}$ it is assumed that no condensation occurs. The model relies upon the user specifying $T_{cond-threshold}$ for the heat exchange device rather than attempting to calculate a dew point for the gas stream. Such a calculation would be complicated by the fact that the gas is pressurized (which affects the calculation of the dew point) and that it is unlikely that the user could specify sufficient data in order for the gas pressure to be calculated under various operating points.

The $hx_{l,i}$ coefficients and $T_{cond-threshold}$ in equation II-50 can be derived by testing a specific heat exchange device over a range of water inlet and gas inlet temperatures and by measuring the heat transfer and by measuring (or calculating based upon the measured fuel flow rate and air inlet flow rate) the gas composition. It is worth noting that tests must be conducted in both the sensible and condensing regimes in order to separately derive the $hx_{s,i}$ coefficients of equation II-45 and the $hx_{l,i}$ coefficients and $T_{cond-threshold}$.

8. Cooling system for PEMFC stack

The PEMFC stack temperature has to be controlled with an internal heat exchanger. The heat that must be extracted from the stack (q_{s-cool}) can be expressed as an empirical function of the stack temperature (T_{stack}) and P_{el},

$$q_{s-cool} = \left[r_0 + r_1 \cdot (T_{stack} - T^0_{stack}) \right] \cdot \left[1 + r_2 \cdot P_{el} + r_3 \cdot {P_{el}}^2 \right] \cdot P_{el} \qquad \text{(II-51)}$$

T^0_{stack} is the nominal stack temperature and T_{stack} the actual stack temperature. Both are user supplied constant values.

An external heat exchanger is used to transfer the thermal energy rejected from the stack to a heat recovery water loop which can provide useful thermal output for cogeneration purposes (see Figure II-2). If this heat exchanger is unable to transfer all of the heat that must be rejected by the stack, then the remaining energy is rejected to the ambient through an air cooler. A bypass loop controls the flow of water through the external heat exchanger. This bypass loop diverts flow through the heat exchanger when conditions are such that the full flow rate of water would result in excess cooling.

The PEMFC's internal heat exchanger, the external heat exchanger which transfers energy to the heat recovery water loop (including its bypass loop), the air cooler, and the pump which circulates the water through this loop are treated in this section.

Internal heat exchanger

The stack inlet tempertature (state point 21 in Figure II-2) required to achieve the necessary heat rejection from the stack (q_{s-cool}) depends upon the water flow rate and the heat transfer coefficient ((UA)$_{s-cool}$) of the internal stack heat exchanger. Both the water flow rate ($\dot{N}_{s-cool}$) and (UA)$_{s-cool}$ are constant user-supplied values. It is assumed that stack side of the internal heat exchanger is isothermal. With this, the heat exchange can be characterized with the following LMTD relationship,

$$q_{s-cool} = (UA)_{s-cool} \cdot \frac{T_{s-cool,out} - T_{s-cool,in}}{\ln\left(\frac{T_{stack} - T_{s-cool,in}}{T_{stack} - T_{s-cool,out}} \right)} \qquad \text{(II-52)}$$

Where $T_{s-cool,in}$ is the stack inlet temperature (state point 21 in Figure II-2) and $T_{s-cool,out}$ is the stack outlet temperature (state point 22 in Figure II-2).

The energy balance of the internal heat exchanger can be given by,

$$q_{s-cool} = (\dot{N}\hat{c}_P)_{s-cool} \cdot (T_{s-cool,out} - T_{s-cool,in}) \qquad \text{(II-53)}$$

Equating the right hand sides of equations II-52 and II-53, rearranging, and taking the exponential of each side leads to,

$$\frac{T_{stack} - T_{s-cool,in}}{T_{stack} - T_{s-cool,out}} = \exp\left[\frac{(UA)_{s-cool}}{(\dot{N}\hat{c}_P)_{s-cool}}\right] \tag{II-54}$$

By substituting $T_{s-cool,in}$ from equation II-53, equation II-54 can be rearranged to express $T_{s-cool,out}$,

$$T_{s-cool,out} = T_{stack} + \frac{1}{1 - \exp\left(\frac{(UA)_{s-cool}}{(\dot{N}\hat{c}_P)_{s-cool}}\right)} \cdot \frac{q_{s-cool}}{(\dot{N}\hat{c}_P)_{s-cool}} \tag{II-55}$$

And $T_{s-cool,in}$ can be evaluated by rearranging equation II-53,

$$T_{s-cool,in} = T_{s-cool,out} - \frac{q_{s-cool}}{(\dot{N}\hat{c}_P)_{s-cool}} \tag{II-56}$$

As mentioned above, $(UA)_{s-cool}$ is a constant user-supplied value. It could be determined using measured stack inlet and outlet temperatures for the known stack temperature and water flow rate using equation II-54.

External heat exchanger

The energy balance of the external heat exchanger is given by,

$$q_{s-cogen} = (\dot{N}\hat{c}_P)_{s-cool} \cdot (T_{s-cool,out} - T_{air-cooler,in}) \tag{II-57}$$

$$= (\dot{N}\hat{c}_P)_{s-cogen} \cdot (T_{s-cogen,out} - T_{s-cogen,in})$$

Where $T_{s-cool,out}$ and $T_{air-cooler,in}$ are the temperatures in the stack cooling water loop (state points 22 and 23 in Figure II-2) and $T_{s-cogen,in}$ and $T_{s-cogen,out}$ are the temperatures in the heat recovery loop (state points 25 and 26 in Figure II-2).

Through the use of $T_{air-cooler,in}$, equation II-57 implicitly considers the effect of the bypass loop and its control. The position of the bypass valve determines the fraction of the stack cooling loop water that flows through the external heat exchanger and the fraction that bypasses the heat exchanger. This valve is actuated to partly bypass the heat exchanger when conditions are such that the full flow rate of water would result in excess cooling. Additionally the heat exchanger is completely bypassed in order to prevent from heat transfer in the wrong direction when the water in the heat recovery loop is warmer than in the stack cooling loop. Equation II-57 accurately expresses the energy balance regardless of the position of the bypass valve.

An intermediate variable is introduced to calculate the performance of the external heat exchanger, $T_{air-cooler,in,no-bypass}$. This variable represents the temperature that $T_{air-cooler,in}$ would be when all the stack cooling water flows through the external heat exchanger (i.e. when there is no bypass).

The heat transfer that would occur in the external heat exchanger when there is no bypass can be described with the LMTD method,

$$q_{s-cogen} = (UA)_{s-cogen} \cdot \frac{(T_{s-cool,out} - T_{s-cogen,out}) - (T_{air-cooler,in,no-bypass} - T_{s-cogen,in})}{\ln\left(\frac{T_{s-cool,out} - T_{s-cogen,out}}{T_{air-cooler,in,no-bypass} - T_{s-cogen,in}}\right)} \qquad \text{(II-58)}$$

Equation II-58 can be rearranged using the same technique elaborated in Section 7 method 2,

$$T_{air-cooler,in,no-bypass} = \qquad \text{(II-59)}$$

$$\left\{\frac{1 - \frac{(\dot{N}\hat{c}_P)_{s-cool}}{(\dot{N}\hat{c}_P)_{s-cogen}}}{\exp\left[(UA)_{s-cogen} \cdot \left(\frac{1}{(\dot{N}\hat{c}_P)_{s-cool}} - \frac{1}{(\dot{N}\hat{c}_P)_{s-cogen}}\right)\right] - \frac{(\dot{N}\hat{c}_P)_{s-cool}}{(\dot{N}\hat{c}_P)_{s-cogen}}}\right\} \cdot T_{s-cool,out}$$

$$+\left\{\frac{\exp\left[(UA)_{s-cogen} \cdot \left(\frac{1}{(\dot{N}\hat{c}_P)_{s-cool}} - \frac{1}{(\dot{N}\hat{c}_P)_{s-cogen}}\right)\right] - 1}{\exp\left[(UA)_{s-cogen} \cdot \left(\frac{1}{(\dot{N}\hat{c}_P)_{s-cool}} - \frac{1}{(\dot{N}\hat{c}_P)_{s-cogen}}\right)\right] - \frac{(\dot{N}\hat{c}_P)_{s-cool}}{(\dot{N}\hat{c}_P)_{s-cogen}}}\right\} \cdot T_{s-cogen,in}$$

$(UA)_{s-cogen}$ is determined using the technique elaborated in Section 7 method 3. However, in this case $(UA)_{s-cogen}$ is assumed to be dependent only upon the flow rate through the heat recovery loop since the water flow through the stack cooling water loop is assumed to be constant. With this, $(UA)_{s-cogen}$ is determined by,

$$(UA)_{s-cogen} = \left[\frac{1}{(hA)_{s-cogen}} + F_{s-cogen}\right]^{-1} \qquad \text{(II-60)}$$

Where $F_{s-cogen}$ is an adjustment factor (see Section 7 method 3) and also includes the effect of the film heat transfer coefficient on the stack cooling loop side of the heat exchanger.

The heat transfer coefficient in equation II-60 is treated as a function of the water flow rate through the heat recovery loop,

$$h_{s-cogen} = h^0_{s-cogen} \cdot \left(\frac{\dot{N}_{s-cogen}}{\dot{N}^0_{s-cogen}} \right)^{n_s} \tag{II-61}$$

Where $h^0_{s-cogen}$ is the film heat transfer coefficient at the nominal flow rate $\dot{N}^0_{s-cogen}$. These empirical constants as well as the empirical constant n_s are supplied by the user. The user also supplies $A_{s-cogen}$ and the empirical constant $F_{s-cogen}$.

The method elaborated above can also be used to represent a constant value of $(UA)_{s-cogen}$ by setting n_s to zero and appropriately setting the other inputs.

Air cooler and circulation pump

An energy balance can be written for the pump which circulates the stack cooling water through the internal heat exchanger, external heat exchanger, and air cooler,

$$(\dot{N}\hat{c}_P)_{s-cool} \cdot (T_{s-cool,in} - T_{air-cooler,out}) = (1 - \alpha_{stack-pump-heat-loss}) \cdot P_{stack-pump-el} \tag{II-62}$$

Where $T_{s-cool,in}$ is the water temperature at the pump outlet (state point 21 in Figure II-2) and $T_{air-cooler,out}$ is the water temperature at the pump inlet (state point 24 in Figure II-2).

The electrical power consumption of the pump ($P_{stack-pump-el}$) is a user-supplied constant value. $\alpha_{stack-pump-heat-loss}$ is the fraction of the power consumption that is lost to the containing room, and is also a user-supplied constant value.

The required temperature at the air cooler outlet is determined by rearranging equation II-62,

$$T_{air-cooler,out} = T_{s-cool,in} - \frac{(1 - \alpha_{stack-pump-heat-loss}) \cdot P_{stack-pump-el}}{(\dot{N}\hat{c}_P)_{s-cool}} \tag{II-63}$$

The inlet temperature to the air cooler ($T_{air-cooler,in}$) can then be determined with the following relationship which implicitly models the control of the bypass valve and the air cooler,

$$T_{air-cooler,in} = max(T_{air-cooler,in,no-bypass}, T_{air-cooler,out}) \tag{II-64}$$

Where $T_{air-cooler,in,no-bypass}$ is calculated with equation II-59 and $T_{air-cooler,out}$ is calculated with equation II-63.

When the result of equation II-64 is $T_{air-cooler,in,no-bypass}$, this implies that the external heat exchanger cannot (or else is just able to) extract sufficient heat from the stack cooling loop. In this case the air cooler is called upon to reject the remaining heat. When the result of equation

II-64 is $T_{air-cooler,out}$, this implies that the air cooler is shut off and that the bypass valve is modulated to avoid excess heat rejection from the stack cooling loop.

The useful heat recovery from the stack cooling loop and the outlet temperature of the heat recovery loop ($T_{s-cogen,out}$) can then be determined by solving equation II-57.

The heat that must be rejected by the air cooler can then be determined as,

$$q_{s-air} = q_{s-cool} + (1 - \alpha_{stack-pump-heat-loss}) \cdot P_{stack-pump-el} - q_{s-cogen} \quad \text{(II-65)}$$

The electrical power consumption of the air-cooler's fan is given as a function of q_{s-air},

$$P_{s-air-el} = f_0 + f_1 \cdot q_{s-air} + f_2 \cdot q_{s-air}^2 \quad \text{(II-66)}$$

$P_{s-air-el}$ is assumed to be lost to the cooling air. The heat released by the air cooler is therefore,

$$q_{air-cooler} = P_{s-air-el} + q_{s-air} \quad \text{(II-67)}$$

As shown in Figure II-1 and discussed in Section 3, $q_{air-cooler}$ can either be lost to the containing room or can be recovered to heat the FCPM's air intake.

9. Dilution Air System and Heat Recovery Ventilator

Some FC-cogeneration devices, such as Fuel Cell Technologies *beta* design, draw air through the cabinet to control the skin losses to the containing room. This warmed air is mixed with the gases that have been cooled in the gas-to-water heat exchanger (state point 14 in Figure II-2) and then vented to the ambient (state point 17 in Figure II-2). A possible design variant would be to add a heat recovery ventilator (HRV) to capture the heat in this mixed stream and to add it to air that is brought into the building for fresh air ventilation purposes.

This device is shown schematically in Figure II-5. The dilution air system and optional HRV are represented with a single control volume. This single control volume is represented by two sections, however, to facilitate the description of its mathematical model: a mixing section and an HRV section.

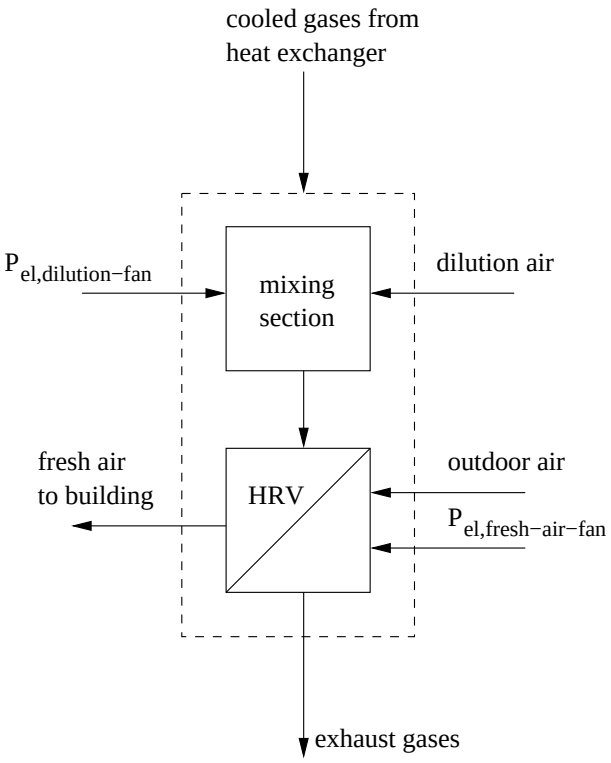

Figure II-5: Schematic of dilution air/HRV system control volume

The following molar balance can be written for the mixing section,

$$\dot{N}_{HX-exh,i} + \dot{N}_{dilution-air,i} = \dot{N}_{HRV-in,i} \tag{II-68}$$

Where equation II-68 applies for each constituent gas (i), e.g. CO_2, H_2O, N_2. $\dot{N}_{HX-exh,i}$ represents the cooled gases that are exhausted from the heat exchanger (state point 14 in Figure II-2).

$\dot{N}_{dilution-air,i}$ represents the dilution air that is drawn from the cabinet (state point 15 in Figure II-2) and $\dot{N}_{HRV-in,i}$ represents the mixed gases that flows into the HRV section (state point 16 in Figure II-2).

It is assumed that the dilution air drawn from the cabinet flows from the room containing the FC-cogeneration device. This can be considered as an unbalanced mechanical exhaust from the room and its impact upon the room's air infiltration rate should be considered in the energy balance of the containing room. The dilution air flow rate, $\dot{N}_{dilution-air}$, is a constant user-specified value (kmol/s).

An energy balance on the mixing section can be written as follows,

$$\dot{H}_{HX\text{-}exh} + \dot{H}_{dilution-air} + P_{el,dilution-fan} = \dot{H}_{HRV\text{-}in} \qquad \text{(II-69)}$$

Where $P_{el,dilution-fan}$ is the AC electrical power supplied to the fan that draws the dilution air from the room. This is treated as a constant user-input value and it is assumed that all of this electrical power is added to the control volume.

The user must also specify the "stack heat loss", that is, the thermal energy transferred from the FCPM to the dilution air ($q_{FCPM-to-dilution}$ in W). This is treated as a constant value.

The enthalpy of the dilution air as it exits the FCPM, but upstream of the fan that draws the dilution air (i.e. the second term on the left side of equation II-69), is determined as follows,

$$\dot{H}_{dilution-air-out} = \dot{H}_{dilution-air-in} + q_{FCPM-to-dilution} \qquad \text{(II-70)}$$

An energy balance can be written for the HRV section as follows,

$$\dot{H}_{HRV-in} + \dot{H}_{OA} + P_{el,fresh-air-fan} = \dot{H}_{exh} + \dot{H}_{vent-air} \qquad \text{(II-71)}$$

Where $\dot{H}_{HRV-in}$ and $\dot{H}_{OA}$ are the enthalpy flow rates into the control volume associated with the gases coming from the mixing section (state point 16 in Figure II-2) and the outdoors (state point 18 in Figure II-2), respectively. $\dot{H}_{exh}$ is the enthalpy flow rate of the gases that are exhausted to the ambient (state point 17 in Figure II-2) and $\dot{H}_{vent-air}$ is the enthalpy flow rate of the warmed ventilation air that is delivered to the building (state point 19 in Figure II-2). $P_{el,fresh-air-fan}$ is the electrical power supplied to the fan that draws the outdoor air through the HRV and supplies it to the building. This is treated as a constant user-input value.

It is assumed that the fresh air fan is located downstream of the heat exchanger area and that all of the electrical power supplied to the fan is added to the control volume. If it is further assumed that the heat capacity of each gas stream remains constant through the heat exchanger and that the heat exchange between the gas streams can be represented with a constant user-specified effectiveness (ε_{HRV}), the heat exchange between the warm gas stream and the fresh air stream can be

given as,

$$q_{HRV} = (\dot{N}\hat{c}_P)_{HRV-in} \cdot (T_{HRV-in} - T_{exh}) \qquad \text{(II-72)}$$

$$= (\dot{N}\hat{c}_P)_{OA} \cdot (T_{vent-air} - T_{OA})$$

$$= \varepsilon_{HRV} \cdot (\dot{N}\hat{c}_P)_{\min} \cdot (T_{HRV-in} - T_{OA})$$

Where $(\dot{N}\hat{c}_P)_{\min}$ is the minimum of $(\dot{N}\hat{c}_P)_{HRV-in}$ and $(\dot{N}\hat{c}_P)_{OA}$ for the current time-step. The outdoor air flow rate is treated as a constant user-specified quantity.

Substituting equations II-72 into equation II-71 yields the following form of the energy balance for the HRV section,

$$T_{vent-air} = \frac{P_{el,\,fresh-air-fan} + \varepsilon_{HRV} \cdot (\dot{N}\hat{c}_P)_{\min} \cdot (T_{HRV-in} - T_{OA})}{\cdot(\dot{N}\hat{c}_P)_{OA}} + T_{OA} \qquad \text{(II-73)}$$

10. Electrical Storage

As SOFCs have slow transient response characteristics it is likely that electrical storage will be used in many SOFC-cogeneration system designs in order to buffer between the SOFC's output and the high-frequency demand transients in the house. The conceptual control strategy between the SOFC, storage, and PCU as outlined in subsection 2.3 requires modelling electricity storage to characterize the charge, discharge, and storage of electrical energy. Storage devices could include capacitors, flywheels, and various types of batteries with lead-acid batteries being the most probable. However, the focus of Annex 42's efforts are on the cogeneration devices themselves and a thorough treatment of storage modelling is considered out of scope.

Therefore, this model specification includes a simple "bucket" model for electrical storage. The user of this specification may prefer to implement more accurate models for specific types of batteries. One such storage model has been implemented into TRNSYS as TYPE185 for lead-acid batteries. This model was developed by Saupe (1993, in German) and described in English (and implemented) by Ulleberg (1998). One category of lead-acid battery models is refered to as "kinetic" such as the model developed by Manwell and McGowan (1993).

The simple electrical storage model described here is a quasi-static, state-of-charge (SOC) model. It is a simple "bucket" model that involves basic accounting of the energy flows and losses to determine the SOC over time. The model does not resolve voltage or current. It assumes power levels are constant over each time step so that energy (joules) is simply power (watts) times the number of seconds in the time step. This is a "constrained-bucket" model in that it includes limits on how much energy can be stored (maximum SOC in Joules), on how much power can be drawn or stored, and accounts for energetic losses from charging or discharging.

The user supplies six inputs for the model including: maximum SOC, $Q_{battery-max}$ (J); maximum rate of charging, $P_{battery-charge-max}$ (W); maximum rate of discharging or drawing, $P_{battery-discharge-max}$ (W); energetic efficiency of charging, ε_{charge} (fraction from 0 to 1 where 1 indicates no losses); energetic efficiency of drawing, $\varepsilon_{discharge}$ (fraction from 0 to 1 where 1 indicates no losses); and intial SOC, $Q_{battery-initial}$ (J) at the beginning of the simulation.

The SOC at the very first time step is determined from user input. At each subsequent time-step of the simulation the battery's SOC is determined based upon its SOC at the previous time-step and the amount of energy drawn or charged. If excess power is available and the battery is being charged, then the SOC is determined by,

$$Q_{battery}^{t+\Delta t} = Q_{battery}^{t} + P_{battery-charge} \cdot \varepsilon_{charge} \cdot \Delta t \qquad \text{(II-74)}$$

Where $Q_{battery}^{t+\Delta t}$ is the battery's SOC, $Q_{battery}^{t}$ is the SOC at the previous time-step, $P_{battery-charge}$ is the power sent to storage, and Δt is the duration of the simulation time-step (seconds). Similarly,

if power needs to be drawn from storage, then the SOC is determined by,

$$Q_{battery}^{t+\Delta t} = Q_{battery}^{t} - \frac{P_{battery-discharge} \cdot \Delta t}{\varepsilon_{discharge}} \tag{II-75}$$

Where $P_{battery-discharge}$ is the power obtained from storage.

The power levels of drawing and charging are first subjected to the limits provided by the user ($P_{battery-charge-max}$ and $P_{battery-discharge-max}$). If the power levels are beyond these limits then they are constrained to the maximum allowable rates.

The balance of energy "lost" during charging and drawing because of energetic losses is represented by $q_{battery-loss}$. As shown in Figure II-1 and discussed in Section 3, $q_{battery-loss}$ can either be lost to the containing room or can be recovered to heat the FCPM's air intake.

If the rate of charging cannot be satisified because either the battery is full or the maximum charging rate would be exceeded, then excess power is exported to the grid. If the rate of drawing cannot be satisified because either the battery is empty or the maximum drawing rate would be exceeded, then power is imported from the grid to meet the requested demand.

The simple constrained-bucket model is an idealization and is not sensitive to much of the behaviour exhibited by real lead-acid batteries. However, it serves to test facets of the fuel cell model and should be helpful for modelling hypothetical systems and in situations where little information is available on the batteries actually used in a particular device.

11. Power Conditioning System

The power conditioning system converts direct current (DC) electricity produced by the FCPM into alternating current (AC) electricity used by most buildings and utility grids. Although power conditioning units are important components in a fuel cell cogeneration device, developing new models for them was considered out of scope for Annex 42's efforts. So a simple approach is used for the treatment of the power losses associated with the PCU which are given by,

$$P_{PCU-losses} = (1 - \eta_{PCU}) P_{PCU-in} \tag{II-76}$$

Where η_{PCU} is the efficiency of the PCU and P_{PCU-in} is the DC electrical power input to the PCU from the FCPM control volume and/or the battery control volume (W). This efficiency is determined with a quadratic curve fit as a function of the power input,

$$\eta_{PCU} = u_0 + u_1 \cdot P_{PCU-in} + u_2 \cdot P_{PCU-in}^2 \tag{II-77}$$

The u_i coefficients are supplied by the user. Empirical data, information from manufacturers, or analytic models can be used to establish these coefficients. A constant efficiency PCU can be modelled simply by setting the coefficients for the first and second order terms to zero.

The power lost in the PCU is converted to heat: $q_{PCU-loss} = P_{PCU-losses}$. As shown in Figure II-1 and discussed in Section 3, $q_{PCU-loss}$ can either be lost to the containing room or can be recovered to heat the FCPM's air intake.

Users of this model specification may also be interested in the second-order approach implemented in TRNSYS TYPE175.

References

Beausoleil-Morrison I., Cuthbert D., Deuchars G., and McAlary G. (2002), "The Simulation of Fuel Cell Cogeneration Systems within Residential Buildings", *Proc. eSim 2002*, 40-47, The Canadian Conference on Building Energy Simulation, Montréal Canada.

Beausoleil-Morrison I. and Kelly N. (2004), "Protocol for Conducting Experiments on Cogeneration Devices", Annex 42 Working Document.

Bove R., Lunghi P., and Sammes N.M. (2005), "SOFC Mathematical Model for Systems Simulations. Part 1: From a Micro-Detailed to Macro-Black-Box Model", *Int J Hydrogen Energy* (30) 181-187.

Braun R.J. (2002), *Optimal Design and Operation of Solid Oxide Fuel Cell Systems for Small-Scale Stationary Applications*, Ph.D. Thesis, University of Wisconsin-Madison, USA.

Chan S.H. and Ding O.L. (2005), "Simulation of a Solid Oxide Fuel Cell Power System Fed by Methane", *Int J Hydrogen Energy* (30) 167-179.

Diethelm R. (2004), "Cheaper, Compacter, and Lighter Through Greater System Integration", *Sulzer Technical Review* 4/2004.

Ferguson A. (2004), 'Control of Residential Combined Cooling, Heating, and Power Systems', *Proc. eSim 2004*, 27-34, The Canadian Conference on Building Energy Simulation, Vancouver Canada.

Gordon S. and McBride B.J. (1971), 'Computer Program for Calculation of Complex Chemical Equilibrium Composition, Rocket Performance, Incident and Reflected Shocks and Chapman-Jouguet Detonations', NASA SP-273.

Haraldsson K. and Wipke K. (2004), "Evaluating PEM Fuel Cell System Models", *Journal of Power Sources*, 126, 88-97.

Karakoussis V., Leach M., van der Vorst R., Hart D., Lane J., Pearson P., and Kilner J. (2000), *Environmental Emissions of SOFC and SPFC System Manufacture and Disposal*, Report F/01/00164/REP to British Department of Trade and Industry.

Kelly N. (2004), *Fuel Cell Model Review for IEA Annex 42*, IEA / ECBCS Annex 42 Working Document, May 2004 Draft.

Manwell J.F. and McGowan J.G. (1993), "Lead Acid Battery Storage Model for Hybrid Energy Systems," *Solar Energy*, Vol. 50(5), 399-405.

Maréchal F. (2004), "Heat Exchanger Calculation", Annex 42 Working Document.

NIST (2003), *Chemistry WebBook*, National Institute of Standards and Technology Standard Reference Database Number 69, March 2003 Release, http://webbook.nist.gov/chemistry/.

Petruzzi L., Cocchi S., Fineschi F. (2003), "A Global Thermo-Electrochemical Model for SOFC Systems Design and Engineering", *Journal of Power Sources*, 118, 96-107.

Reynolds W.C. and Perkins H.C. (1977), *Engineering Thermodynamics*, McGraw-Hill.

Saupe G. (1993), *Photovoltaic Power Supply System with Lead-Acid Battery Storage: Analysis of the Main Problem, System Improvements, Development of a Simulation Model for a Battery* (in German), Ph.D. Thesis, University of Stuttgart, Germany.

Singhal S.C. and Kendall K. (2003), *High Temperature Solid Oxide Fuel Cells: Fundamentals, Design, and Applications*, Elsevier, Oxford UK.

Ulleberg Ø. (1998), *Stand-Alone Power Systems for the Future: Optimal Design, Operation, and Control of Solar-Hydrogen Energy Systems*, Ph.D. Thesis, Norwegian University of Science and Technology, Trondheim Norway.

Appendix A : Coefficients for Shomate Equation

This appendix provides input data for computing thermophysical properties when implementing the fuel cell model. The Shomate formulation used by NIST (see equation II-12) is used with the coefficients listed in Table II-1. Sources of the data are listed with "NIST" indicating that the data are directly from the NIST Chemistry Webbook and "CHEMKIN" indicating that the data were developed by Annex 42 from library data for the CHEMKIN modelling program. The CHEMKIN library data were evaluated using the appropriate polynomial (Gordon and McBride 1971) and then new coefficients determined by fitting the data to equation II-12 using the program MATHEMATICA 4.0 from Wolfram Research, Inc.

	A	B	C	D	E	F	H	Source
N_2	26.092	8.218801	-1.976141	0.159274	0.044434	-7.98923	0.0	NIST
O_2	29.659	6.137261	-1.186521	0.09578	-0.219663	-9.861391	0.0	NIST
Ar	20.786	2.8259E-7	-1.4642E-7	1.0921E-8	-3.6614E-8	-6.19735	0.0	NIST
CO_2	24.99735	55.18696	-33.69137	7.948387	-0.136638	-403.6075	-393.5224	NIST
H_2O (gas)	29.0373	10.2573	2.81048	-0.95914	0.11725	-250.569	-241.8264	CHEMKIN
H_2O (liq)	-203.606	1523.29	-3196.413	2474.455	3.85533	-256.5478	-285.8304	NIST
H_2	33.066178	-11.363417	11.432816	-2.772874	-0.158558	-9.9808	0.0	NIST
CH_4	-0.703029	108.4773	-42.52157	5.862788	0.678565	-76.84376	-74.8731	NIST
C_2H_6	-3.03849	199.202	-84.9812	11.0348	0.30348	-90.0633	-83.8605	CHEMKIN
C_3H_8	-23.1747	363.742	-222.981	56.253	0.61164	-109.206	-103.855	CHEMKIN
C_4H_{10}	-5.24343	426.442	-257.955	66.535	-0.26994	-149.365	-133.218	CHEMKIN
C_5H_{12}	-34.9431	576.777	-338.353	76.8232	1.00948	-155.348	-146.348	CHEMKIN
C_6H_{14}	-46.7786	711.187	-438.39	103.784	1.23887	-176.813	-166.966	CHEMKIN
CH_3OH	14.1952	97.7218	-9.73279	-12.8461	0.15819	-209.037	-201.102	CHEMKIN
C_2H_5OH	-8.87256	282.389	-178.85	46.3528	0.48364	-241.239	-234.441	CHEMKIN

Table II-1: Coefficients for Shomate Equation

Section III: Combustion Engine Based Cogeneration Model Specifications

A Generic Model Specification for Combustion-based Residential Cogeneration Devices

MODEL SPECIFICATION AUTHORS:

Alex Ferguson (Natural Resources Canada)

Nick Kelly (University of Strathclyde)

Acknowledgements

The authors of this report would like to acknowledge the contributions of the following individuals:

- Ian Beausoleil-Morrison Natural Resources Canada)
- Ernst-Jan Bakker (ECN)
- Conrad Gähler (Siemens Building Technologies)
- Brent Griffith (National Renewable Energy Laboratories)
- Andreas Weber (EMPA)
- Ismet Ugursal (Dalhousie University, formerly with University of Victoria)

The assistance of the other members of Annex 42 in producing this report is also gratefully acknowledged.

Introduction

The use of internal combustion engines for small to medium scale combined heat and power (cogeneration) systems is well established world wide. The improved efficiency resulting from combined heat and power generation means that co-generated electricity is often a viable alternative to purchasing power from the grid, especially when there is a consistent, year-round demand for the heat recovered from cooling water and exhaust gases, such as domestic or process hot water loads. Further, in large cogeneration schemes there is intrinsic stability in both heat and power loadings due to the diversity of many individual electrical loads (and hence a distribution of load timings) and thermal load capacitance (e.g. in swimming pools and hot water storage). Economic criteria dictate that there is a close match between the heat and power characteristics (often termed the heat to power ratio – H:P) of the cogeneration unit and the loads it serves.

Micro cogeneration is a much more recent innovation, with technologies such as Stirling engines (SE), micro turbines, fuel cells and internal combustion engines (ICE) just beginning to emerge. Dentice d'Accadia et al. (2003) define micro-cogeneration devices as those delivering 15 kW of electrical power or less. Micro-cogeneration engine units have significantly different characteristics to those of the small-to-medium cogeneration devices commonly used in larger buildings. They are typically fueled using lower octane liquid and gaseous fuels such as natural gas, petrol or LPG. Heat to power ratios vary significantly, ranging from nearly 1:1 for some fuel cell technologies to as high as 10:1 for external combustion (Stirling) engines (Larminie and Dicks 2001, WhisperTech 2002).

While fuel cell based micro-cogeneration technology remains at the prototype stage, the development of ICE and SE based units has progressed rapidly in recent years[6]. Dentice d'Accadia et al. (2003) describe 12 different combustion engine micro-cogeneration units, with sizes ranging from 1-15 kW of electrical output and 3-39 kW of thermal output. These devices vary from single cylinder to four cylinder configurations driving a

[6] The major difference between the Stirling engine and the more common internal combustion engine is that combustion is *external* to the gas inside the cylinder.

variety of generator types that supply both single and three phase power. Both Honda and SenerTec presently market residential-scale ICE-based cogeneration devices (Honda 2004, Zilch 2005), and SE-based cogeneration devices are being produced by in Germany and New Zealand (Solo Stirling GmbH 2003, Whisper Tech 2002).

In support of Annex 42's modelling objectives models for ICE and SE devices were developed independently by Kelly (2005) and Ferguson (2005) respectively. Early versions of these models disaggregated SE and ICE devices into a set of control volumes representing the functional components (e.g. heat exchanger) within these systems, and used parametric equations to describe the behaviour within each subcomponent. However, discussions with Annex 42 participants performing experimental characterization of micro cogeneration devices indicated that the empirical data necessary to calibrate such models could only be obtained through invasive measurements, which were beyond the scope of the tests being undertaken. The authors concluded that such models would therefore be of limited value to the modelling community and so would not be developed further. The ICE and SE models subsequently evolved towards more practical representations requiring less detailed experimental characterization. Both models abandoned detailed characterization of combustion and heat transfer processes occurring within the engines in favour of empirical-based "performance maps." The models instead focused on the heat recovery processes within the devices and their interaction with other systems within the building.

These revised models were presented by Kelly (*ibid*) and Ferguson (*ibid*) at the September 2005 Annex 42 meeting in Munich. Noting the similarities between them, the Annex participants decided to merge the models into a single specification.

The result, presented in this section, is a general model specification, which is particularly suited to the modelling of combustion-based cogeneration devices such as SE and ICE units, but is applicable to any device simultaneously producing heat and power from which heat is recovered as hot water.

The model specification uses empirical data contained within a "performance map" to represent device-specific performance characteristics coupled with thermally massive elements to characterize the device's dynamic thermal performance. This approach has

significant advantages over the detailed modelling approach adopted in the early stages of the project: the simplicity of the model; ease of calibration and reduced data collection burden. However, there are also disadvantages:

- The model relies almost entirely on empirical data, though the structure reflects the underlying physical processes.
- Once calibrated, the performance map component of the model is applicable to only one engine and fuel type, and each new cogeneration device must be characterized in a laboratory environment before its performance can be accurately simulated.

Whilst the performance map itself is intrinsically non-generic, the generic form of the model and the approach described here for incorporating the model into a building simulation tool will be suitable for all the codes utilized within Annex 42.

1 Modelling Strategy

The energy and mass flows in ICE or SE-based cogeneration devices comprise:

- convective and radiant heat release from combustion of fuel in air;
- convective heat transfer with the flow of reactant and product gases, and coolant;
- energy storage in the engine block and other thermally massive components;
- conductive heat transfer across heat exchangers, and possible latent heat recovery from the combustion gases;
- mechanical shaft power produced by the engine, and used by fluid-handling equipment; and
- electrical power produced by the system's alternator, and used by the system's electric motors to drive fluid handling equipment.

During the operation of an ICE or SE cogeneration device, energy is converted between thermo-chemical, thermo-fluid, mechanical and electrical domains.

However for the generalized model topology proposed in this section, many of the energy exchanges described are captured in the performance map, and only those energy exchanges that interact with other balance of plant components are of interest. This

modelling approach therefore aggregates the internal energy exchanges into two empirical correlations that describe the system's part-load electrical and thermal efficiencies.

2 Model Topology

Three control volumes are used to model the cogeneration unit dynamic thermal characteristics:

- the *energy conversion control volume* represents the engine working fluid, combustion gases and engine alternator, this control volume feeds information from the engine unit performance map (in the form of a heat flux) into the thermal model;
- the *thermal mass control volume* represents the aggregated thermal capacitance associated with the engine block and the majority of the heat exchanger shells; and
- the *cooling water control volume* represents the cooling water flowing through the device and the elements of the heat exchanger in immediate thermal contact.

The energy flows between these control volumes are depicted in Figure III-1.

2.1 Model Constituents

2.1.1 Energy conversion control volume

The steady-state energy balance for the energy conversion control volume is:

$$\dot{H}_{fuel} + \dot{H}_{air} = P_{net,ss} + q_{gen,ss} + \dot{H}_{exh} \qquad \text{(III-1)}$$

where:

$\dot{H}_{fuel}$ is the total enthalpy of the fuel,

$\dot{H}_{air}$ is the total enthalpy of the combustion air,

$P_{net,ss}$ is the rate of steady-state electricity production,

$q_{gen,ss}$ is the rate steady-state heat production, and

$\dot{H}_{exh}$ is the total enthalpy of the exhaust gases.

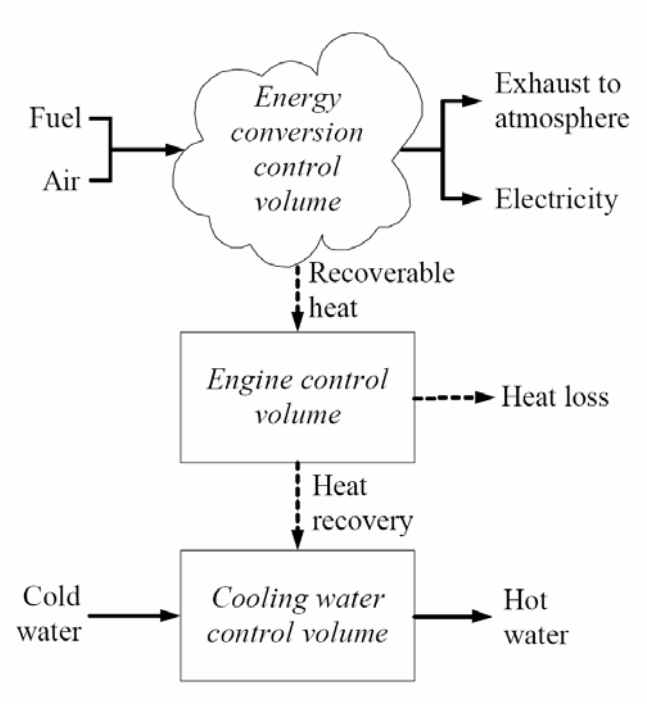

Figure III-1: combustion cogeneration model control volumes

The model does not attempt to fully characterize the energy balance described by Equation III-1. Instead, the engine's steady-state (part load) performance is correlated to the total energy input to the system:

$$P_{net,ss} = \eta_e q_{gross} \tag{III-2}$$

$$q_{gen,ss} = \eta_q q_{gross} \tag{III-3}$$

$$q_{gross} = \dot{m}_{fuel} \cdot LHV_{fuel} \tag{III-4}$$

where:

q_{gross} is the gross heat input into the system (W),

$\dot{m}_{fuel}$ is the fuel flow rate (kg/s or kmol/s),

LHV_{fuel} is the lower heating value of the fuel used by the system (J/kg or J/kmol),

$P_{net,ss}$ is the steady-state electrical output of the system (W),

η_e is the steady-state electrical conversion efficiency of the engine (-),

$q_{gen,ss}$ is the steady-state rate of heat generation within the engine (W), and

η_q is the steady-state part load, thermal efficiency of the engine (-).

Due to the effects of thermal storage, heat losses and internal controls within the cogeneration system, the actual rates of power delivery and heat recovery (P_{net} and q_{HX}) may differ from the steady-state rates described in Equations III-2 and III-3. Calculation of the dynamic power delivery will be discussed in Section 5, while calculation of dynamic heat recovery is discussed in sections 2.1.2 to 2.1.4.

The lower-heating value of the fuel is determined by summing the enthalpies of formation of all reactants and products, and assuming that all of the water in the combustion products is in vapour form:

$$LHV_{fuel} = \frac{\sum_{reactants} \chi_i \hat{h}_i^o - \sum_{products} \chi_i \hat{h}_i^o}{\sum_{reactants} M_i} \qquad \text{(III-5)}$$

where:

χ_i is the molar fraction of constituent *i*, (-)

$\hat{h}_i^o$ is the enthalpy of formation of constituent *i* at standard temperature and pressure (J/kg or J/kmol), and

M_i is the molar mass of constituent *i*. (kg/kmol)

The enthalpies of formation ($\hat{h}_i^o$) should be evaluated at 25°C for all constituents. The model should, at minimum, support the fuel constituents given in Table III-1. This constituent list is intended to support specification of gaseous fuels, such as natural gas. While some micro-cogeneration devices may run on liquid fuels such as gasoline or diesel, the model specification does not support explicit modelling of the various additives that may affect the heating value of these fuels. Instead, the model allows for a "generic liquid fuel", whose empirically measured heating value is provided by the user.

Table III-1: Fuel constituents

Compound	Chemical Formula
Hydrogen	H_2
Methane	CH_4
Ethane	C_2H_6
Propane	C_3H_8
Butane	C_4H_{10}
Pentane	C_5H_{12}
Methanol*	CH_3OH
Ethanol*	C_2H_5OH
Carbon monoxide	CO
Carbon dioxide	CO_2
Nitrogen	N_2
Oxygen	O_2
Generic liquid fuel**	—

Notes:

* CH_3OH and C_2H_5OH are assumed to be in a vapour state

** The model should permit specification of a generic liquid fuel, along with and empirically derived heating value

2.1.2 Engine control volume

The dynamic thermal behaviour of the combustion-based cogeneration device is characterized by the thermal mass of its engine block and encapsulated working fluid, internal heat exchange equipment, and in the case of SE-based technology, the external heater.

Since the model lacks the resolution required to characterize the thermal response of these individual subcomponents, it is assumed that they can be represented using a single, homogeneous *engine control volume*. The thermal energy stored within this control volume is quantified using an aggregate thermal capacitance, $[MC]_{eng}$, (J/K) and an equivalent average engine temperature T_{eng} (^{o}C)

The energy balance of the engine control volume is:

$$[MC]_{eng}\frac{dT_{eng}}{dt} = q_{gen,ss} - q_{HX} - q_{skin-loss} \qquad \text{(III-6)}$$

where:

$[MC]_{eng}$ is the thermal capacitance of the control volume (W/K),

q_{HX} is the rate of heat transfer to the cooling water (W),

$q_{skin-loss}$ is the rate of heat loss from the unit (W),

T_{eng} is the bulk temperature of the thermal mass control volume (^{o}C), and

t is time.

2.1.3 Cooling water control volume

The energy balance of the cooling water control volume is:

$$[MC]_{cw}\frac{T_{cw,o}}{dt} = [\dot{m}c_p]_{cw}\left(T_{cw,i} - T_{cw,o}\right) + q_{HX} \qquad \text{(III-7)}$$

where:

$[MC]_{cw}$ is the thermal capacitance of the encapsulated cooling water and heat exchanger shell in immediate thermal contact (J/K),

$T_{cw,o}$ is the bulk exit temperature of the encapsulated cooling water and shell (^{o}C),

$T_{cw,i}$ is the temperature of the cooling water entering the unit (^{o}C), and

$[\dot{m}c_p]_{cw}$ is the thermal capacity flow rate associated with the cooling water (W/K).

2.1.4 Heat transfer

Heat is transferred to the cooling water from the exhaust gases and the engine casing. The rate of heat recovery may differ from the calculated steady-state rate of recoverable heat production ($q_{gen,ss}$) due to:

- the thermal mass of the engine and other heat transfer components , which store some of the recoverable heat produced within the engine, and
- the effects of internal controllers regulating phenomena such as of exhaust-gas recirculation and the operation of the external heater in Stirling engines.

The model assumes the dynamic thermal behaviour of the combustion cogeneration device is attributable to the thermal mass of the engine, exhaust-gas heat exchanger and, in Stirling engines, the external heater.

The model assumes the heat transfer to the cooling water is proportional to the difference in the temperature of cooling water control volume and the engine control volume temperature.

The heat transfer between the engine and the cooling water control volume is quantified using an overall heat-transfer coefficient:

$$q_{HX} = UA_{HX}\left(T_{eng} - T_{cw,o}\right) \qquad \text{(III-8)}$$

where UA_{HX} (W/K) is the overall thermal conductance between the engine cooling water control volumes, and T_{eng} (^{o}C) is the average temperature of the engine control volume.

It is assumed that the heat lost from the engine is proportional to the temperature difference between the engine control volume and the surroundings. Thus:

$$q_{skin-loss} = UA_{loss}\left(T_{eng} - T_{room}\right) \quad \text{(III-9)}$$

where UA_{loss} (W/K) is the effective thermal conductance between the engine control volume and the surroundings.

Using Equations III-8 and III-9, the engine and cooling water control volume energy balance equations (Equations III-6 and III-7) can be rewritten:

$$[MC]_{eng}\frac{dT_{eng}}{dt} = UA_{HX}\left(T_{cw,o} - T_{eng}\right) + UA_{loss}\left(T_{room} - T_{eng}\right) + q_{gen,ss} \quad \text{(III-10)}$$

$$[MC]_{cw}\frac{T_{cw,o}}{dt} = [\dot{m}c_p]_{cw}\left(T_{cw,i} - T_{cw,o}\right) + UA_{HX}\left(T_{eng} - T_{cw,o}\right) \quad \text{(III-11)}$$

2.2 Part load performance

The cogeneration system's part load electrical and thermal efficiencies, (η_e, η_q [-]), are determined using empirical correlations relating the conversion efficiencies to the flow rate and temperature of cooling water, and the unit's electrical loading:

$$\eta_e = f(\dot{m}_{cw}, T_{cw}, P_{net,ss}) \quad \text{(III-12)}$$

$$\eta_q = f(\dot{m}_{cw}, T_{cw}, P_{net,ss}) \quad \text{(III-13)}$$

where:

$\dot{m}_{cw}$ is the mass flow rate of the cooling water (kg/s), and

T_{cw} is the temperature of the cooling water at the inlet of the cooling water control volume (^{o}C).

Together, these correlations constitute a "performance map" describing the cogeneration system's steady-state behaviour under a variety of loading conditions.

The system's dynamic thermal response can differ from the operating point predicted by the performance map due to the effects of thermal mass, while the available electrical

output is often governed by internal control constraints. The model's treatment of these effects is discussed later .

Experimental data collected from the system may indicate that a particular functional form is well suited to the correlations. Until then, it is proposed to use tri-variate polynomials truncated above 2nd order:

$$\begin{aligned}\eta_e = {} & a_0 + a_1 P_{net,ss}^2 + a_2 P_{net,ss} \\ & + a_3 \dot{m}_{cw}^2 + a_4 \dot{m}_{cw} \\ & + a_5 T_{cw}^2 + a_6 T_{cw} \\ & + a_7 P_{net,ss}^2 \dot{m}_{cw}^2 + a_8 P_{net,ss} \dot{m}_{cw} + a_9 P_{net,ss} \dot{m}_{cw}^2 + a_{10} P_{net,ss}^2 \dot{m}_{cw} \\ & + a_{11} P_{net,ss}^2 T_{cw}^2 + a_{12} P_{net,ss} T_{cw} + a_{13} P_{net,ss} T_{cw}^2 + a_{14} P_{net,ss}^2 T_{cw} \\ & + a_{15} \dot{m}_{cw}^2 T_{cw}^2 + a_{16} \dot{m}_{cw} T_{cw} + a_{17} \dot{m}_{cw} T_{cw}^2 + a_{18} \dot{m}_{cw}^2 T_{cw} \\ & + a_{19} P_{net,ss}^2 \dot{m}_{cw}^2 T_{cw}^2 + a_{20} P_{net,ss}^2 \dot{m}_{cw}^2 T_{cw} + a_{21} P_{net,ss}^2 \dot{m}_{cw} T_{cw}^2 + a_{22} P_{net,ss} \dot{m}_{cw}^2 T_{cw}^2 \\ & \quad + a_{23} P_{net,ss}^2 \dot{m}_{cw} T_{cw} + a_{24} P_{net,ss} \dot{m}_{cw}^2 T_{cw} + a_{25} P_{net,ss} \dot{m}_{cw} T_{cw}^2 \\ & \quad + a_{26} P_{net,ss} \dot{m}_{cw} T_{cw}\end{aligned} \tag{III-14}$$

$$\begin{aligned}\eta_q = {} & b_0 + b_1 P_{net,ss}^2 + b_2 P_{net,ss} \\ & + b_3 \dot{m}_{cw}^2 + b_4 \dot{m}_{cw} \\ & + b_5 T_{cw}^2 + b_6 T_{cw} \\ & + b_7 P_{net,ss}^2 \dot{m}_{cw}^2 + b_8 P_{net,ss} \dot{m}_{cw} + b_9 P_{net,ss} \dot{m}_{cw}^2 + b_{10} P_{net,ss}^2 \dot{m}_{cw} \\ & + b_{11} P_{net,ss}^2 T_{cw}^2 + b_{12} P_{net,ss} T_{cw} + b_{13} P_{net,ss} T_{cw}^2 + b_{14} P_{net,ss}^2 T_{cw} \\ & + b_{15} \dot{m}_{cw}^2 T_{cw}^2 + b_{16} \dot{m}_{cw} T_{cw} + b_{17} \dot{m}_{cw} T_{cw}^2 + b_{18} \dot{m}_{cw}^2 T_{cw} \\ & + b_{19} P_{net,ss}^2 \dot{m}_{cw}^2 T_{cw}^2 + b_{20} P_{net,ss}^2 \dot{m}_{cw}^2 T_{cw} + b_{21} P_{net,ss}^2 \dot{m}_{cw} T_{cw}^2 + b_{22} P_{net,ss} \dot{m}_{cw}^2 T_{cw}^2 \\ & \quad + b_{23} P_{net,ss}^2 \dot{m}_{cw} T_{cw} + b_{24} P_{net,ss} \dot{m}_{cw}^2 T_{cw} + b_{25} P_{net,ss} \dot{m}_{cw} T_{cw}^2 \\ & \quad + b_{26} P_{net,ss} \dot{m}_{cw} T_{cw}\end{aligned} \tag{III-15}$$

Where a_0–a_{26} (-) and b_0–b_{26} (-) are empirically-derived coefficients. It is likely that the value of many of these coefficients will reduce to zero after regression analysis, however they have been included for completeness.

Note that the efficiency correlations described by Equations III-14 and III-15 quantify the cogeneration system's steady-state and part load performance, and do not characterize its dynamic thermal or electrical behaviour. In reality, the thermal mass of the system will limit the rate at which the system's operating point can be changed. Furthermore, internal, low-level controls may restrict the rates at which the fuel flow to the system and the power produced by the system are changed.

2.3 Cooling water flow rate

Some ICE- and SE-based cogeneration devices are equipped with an internal valve used to vary the hydraulic resistance through the cooling water circuit. These devices can effectively regulate the flow rate of the cooling water loop to optimize engine performance and heat recovery (Zilch, 2005)

In these devices, the cooling water flow rate is not imposed on the unit by the balance of plant configuration, but instead is chosen by the unit's internal controls. Since these controls are not directly modelled, their effects must be aggregated into the system performance map. Therefore, an additional empirical correlation is required for devices with internal control of the cooling water flow rate (kg/s):

$$\begin{aligned}\dot{m}_{cw} = {} & c_0 + c_1 P_{net,ss}^2 + c_2 P_{net,ss} \\ & + c_3 T_{cw}^2 + c_4 T_{cw} \\ & + c_5 P_{net,ss}^2 T_{cw}^2 + c_6 P_{net,ss} T_{cw} + c_7 + c_8 P_{net,ss}^2 T_{cw}\end{aligned} \qquad \text{(III-16)}$$

2.4 Combustion air flow

The air flow into the unit does not effect the model's thermal or electrical performance predictions. However, if the cogeneration unit draws its combustion air from its surrounding enclosure, the induced air flow will have a significant effect on the building infiltration and must be accounted for by the building simulation environment.

The air stoichiometry is regulated to manage the cogeneration unit's combustion efficiency, operating temperature and emissions. Since the single control volume used to

model the engine and auxiliary equipment does not provide adequate resolution to quantify these effects, the unit's combustion air flow rate to the system fuel flow:

$$\begin{aligned} \dot{m}_{air} &= f(\dot{m}_{fuel}) \\ &= d_0 + d_1 \dot{m}_{fuel}^2 + d_2 \dot{m}_{fuel} \end{aligned} \tag{III-17}$$

where $\dot{m}_{air}$ is the combustion air flow rate (kg/s).

2.5 Changing operating points

Low-level controllers may restrict the rates at which the fuel flowing to the system can be increased and decreased[7]. In the absence of detailed data describing these controllers, the model allows constraints on the maximum rate of change permitted in the system fuel flow using empirically derived data as follows:

$$\frac{d\dot{m}_{fuel}}{dt} = \frac{\left| \dot{m}_{fuel,demand}^{t+\Delta t} - \dot{m}_{fuel}^{t} \right|}{\Delta t} \tag{III-18}$$

where:

$\dot{m}_{fuel,demand}^{t+\Delta t}$ is the system fuel flow rate requested by a high-level control (kg/s), and

t is time (s), and Δt is the duration of the simulation time step (s).

The fuel flow rate requested from the cogeneration unit can then be adjusted to reflect the unit's embedded internal controller characteristics:

$$\dot{m}_{fuel}^{t+\Delta t} = \begin{cases} \dot{m}_{fuel,demand}^{t+\Delta t} & \text{if } d\dot{m}_{fuel}/dt \le \left(d\dot{m}_{fuel}/dt\right)_{max} \\ \dot{m}_{fuel}^{t} \pm \left(d\dot{m}_{fuel}/dt\right)_{max} & \text{if } d\dot{m}_{fuel}/dt > \left(d\dot{m}_{fuel}/dt\right)_{max} \end{cases} \tag{III-19}$$

where $\dot{m}_{fuel}^{t} \pm \left(d\dot{m}_{fuel}/dt\right)_{max}$ is the maximum rate of change in the system fuel flow rate permitted by the low-level controller (kg/s).

---

[7] The fuel flow rate may be managed to optimize other engine performance criteria. For instance, in modulating Stirling CHP, the system's operating point is actually regulated by varying the pressure of the working fluid inside the engine. A low-level controller then regulates the fuel flow to ensure the temperature at the hot-end of the engine is maintained within an efficient operating range. Since the Stirling power system control volume does not provide sufficient resolution to model these effects, the fuel flow rate is used to uniquely describe the system operating point, and is defined as the system's principle control parameter

The dynamic response of the cogeneration system's power delivery depends on the constraints on the system's fuel flow rate, its thermal mass, the energy use of other auxiliary electrical equipment and the action of any embedded control devices. Since the model does not characterize these effects, the user may optionally constrain the unit's predicted dynamic electric response using empirical data. Changes in the system's electrical output can be described using a linear derivative:

$$\frac{dP_{net}}{dt} = \frac{\left| P_{net,ss}^{t+\Delta t} - P_{net}^{t} \right|}{\Delta t} \tag{III-20}$$

where P_{net} (W) is the system's power delivery under steady-state conditions.

The rate of change in the cogeneration system's power output is compared to the maximum rate of change derived from empirical data, and adjusted to reflect the unit's transient characteristics:

$$P_{net}^{t+\Delta t} = \begin{cases} P_{net,ss}^{t+\Delta t} & \text{if } dP_{net}/dt \le \left(dP_{net}/dt\right)_{max} \\ P_{net}^{t} \pm \left(dP_{net}/dt\right)_{max} & \text{if } dP_{net}/dt > \left(dP_{net}/dt\right)_{max} \end{cases} \tag{III-21}$$

where $\left(dP_{net}/dt\right)_{max}$ (W/s) is the maximum rate of change in the system's electrical output.

Empirical data may show that thermal mass and heat transfer have the greatest impact on the system's electrical response, and an exponential decay function is better suited to represent the dynamic behaviour of the system's electrical output. Equations III-19 and III-21 will be revisited when detailed validation data is available.

2.5.1 Deactivating rate of change limits

To preserve the flexibility of the model, developers should add inputs permitting the deactivation of the fuel flow and power generation rate of change limits.

3 Modes of operation

Section 2 discussed the characterization of cogeneration systems when operating normally (henceforth called the *normal operation* mode). However, cogeneration systems

may exhibit three other operating modes with markedly different characteristics. These are the standby, warm-up and cool-down modes of operation.

3.1 Standby

When no electric or thermal output is requested, the unit is assumed to be in standby mode. During standby operation, the unit consumes no fuel and produces no heat. However, the electronic controllers within the unit require some electricity while awaiting activation. Thus:

$$\begin{aligned} P_{net} &= P_{net,standby} \\ Q_{gen,ss} &= 0 \\ \dot{m}_{fuel} &= 0 \end{aligned} \qquad \text{(III-22)}$$

where $P_{net,standby}$ (W) is the power used by the unit's control systems while in standby operation. The model's thermal response is then characterized by solving Equations III-10 and III-11.

3.2 Warm-up

Once activated, Stirling engines may exhibit a warm-up period, in which the fuel flow and electric output differ considerably from their steady-state values. The following mechanisms govern the unit's operation during warm-up.

- The heater and the engine's "hot end" do not reach their operational temperature instantly. Without sufficient heat transfer to the engine, the requested power cannot be produced.
- The unit's controller may increase the fuel flow to the heater to raise the heater temperature as quickly as possible, permitting delivery of the requested power sooner.

Treatment of the warm-up period differs between Stirling and internal combustion engines.

3.2.1 Stirling engines

The warm-up characteristics of Stirling engines are correlated to a *nominal engine temperature*, which is assumed to represent conditions in the engine under steady-state conditions. During the warm-up period, it is assumed that:

- the engine's controller adjusts the engine fuel flow to the value corresponding to its maximum steady-state power output, and
- the engine's controller further increases this value by an amount inversely proportional to the difference between the nominal engine temperature and the actual engine temperature.

Therefore, the engine's fuel flow during warm-up is:

$$\dot{m}_{fuel,warm-up} = \dot{m}_{fuel,ss-max} + k_f \dot{m}_{fuel,ss-max}\left(\frac{T_{eng,nom} - T_{room}}{T_{eng} - T_{room}}\right) \qquad \text{(III-23)}$$

where $\dot{m}_{fuel,warm-up}$ (kg/s) is the rate of fuel flow during warm-up, $\dot{m}_{fuel,ss-max}$ (kg/s) is the maximum rate of fuel flow to the device under steady-state conditions, k_f is an empirical coefficient, and $T_{eng,nom}$ (^{o}C) is s the nominal engine temperature. The maximum fuel flow under steady-state conditions ($\dot{m}_{fuel,ss-max}$) (kg/s) is not a model input, but can be determined by solving equations III-2, III-4 and III-5 with $P_{net,ss}=P_{max}$.

If the cogeneration unit has been inactive for extended periods, the engine control volume temperature (T_{eng}) may approach that of the enclosure (T_{room}). Under these conditions, the calculated warm-up fuel flow rate, $\dot{m}_{fuel,warm-up}$, can grow very large. Indeed, if the control volume and enclosure temperatures are equal, evaluation of Equation III-23 may result in an overflow error. Under these circumstances, the warm-up fuel flow is limited by an empirical ratio:

$$\dot{m}_{fuel,max,warm-up} = \begin{cases} \dot{m}_{fuel,warm-up} & \text{if } \dot{m}_{fuel,warm-up} \le r_{fuel,warm-up}\dot{m}_{fuel,ss-max} \\ r_{fuel,warm-up}\dot{m}_{fuel,ss-max} & \text{if } \dot{m}_{fuel,warm-up} > r_{fuel,warm-up}\dot{m}_{fuel,ss-max} \end{cases} \qquad \text{(III-24)}$$

where $r_{fuel,warm-up}$ describes the ratio between the maximum fuel flow during the warm-up period, and that observed under steady-state operation.

In the unlikely event that the enclosure temperature (T_{room}) exceeds the nominal engine temperature ($T_{eng,nom}$), the warm-up period fuel flow correlation (Equation III-24) is no longer valid. Under these circumstances, the model should take one of two actions:

- If the engine temperature is greater than the nominal engine temperature ($T_{eng}>T_{eng,nom}$), the unit should be switched into normal operation.
- Otherwise, the warm-up fuel flow rate should be set to the unit's maximum steady-state value ($\dot{m}_{fuel,warm-up} = \dot{m}_{fuel,ss-max}$), and a warning should be issued to the user.

The rate of heat generation within the engine during warm-up is determined by evaluating Equation III-3, using the steady-state heat generation efficiency, η_q. The model's thermal response is then characterized by solving Equations III-10 and III-11.

The actual power produced during warm-up is also correlated to the nominal temperature:

$$P_{net,warm-up} = P_{max} k_p \left(\frac{T_{eng} - T_{room}}{T_{eng,nom} - T_{room}} \right) \qquad \text{(III-25)}$$

where $P_{net,warm-up}$ (W) is the rate of power generation during warm-up, and k_p is an empirical coefficient.

The denominator in Equation III-25 may be equal-to or less-than zero in the unlikely event that $T_{eng,nom} \leq T_{room}$. The warm up power production is not valid under these circumstances, and the model should take one of two actions:

- If the engine temperature is greater than the nominal engine temperature ($T_{eng}>T_{eng,nom}$), the unit should be switched into normal operation.
- Otherwise, the warm-up period power output should be set to the unit's maximum value ($P_{net,warm-up}=P_{max}$), and a warning should be issued to the user.

The Stirling engine transitions from warm-up to normal operation whenever i) the engine temperature exceeds the nominal value (ie. $T_{eng}>T_{eng,nom}$) or the net power produced exceeds that requested by the controller (ie. $P_{net,warm-up} > P_{demand}$).

3.2.2 Internal combustion engines

The start-up characteristics of internal combustion engines are not sensitive to engine temperature. However, these devices may exhibit a static time delay between activation of the unit and power generation. The power generated by these devices is determined as:

$$P_{net,warm-up} = \begin{cases} 0 & \text{if } (t - t_o) < t_{warm-up} \\ P_{demand} & \text{if } (t - t_o) \geq t_{warm-up} \end{cases} \quad \text{(III-26)}$$

where t is the current time (s) and t_o (s) is the time at which the engine was started . The parameter $t_{warm-up}$ (s) describes the static delay between activation and power generation.

The fuel flow is determined during warm-up by solving Equations III-2, III-4 and III-5, using the steady state electrical efficiency, η_q, and setting the steady-state power generation to the demand specified by the controller ($P_{net,ss} = P_{demand}$).

The rate of heat generation within the engine during warm-up is determined by evaluating Equation III-3, using the steady-state heat generation efficiency, η_q. The model's thermal response is then characterized by solving Equations III-10 and III-11.

Once the specified static delay has lapsed (ie $t - t_o \geq t_{warm-up}$), the warm-up period is complete and the unit switches to normal operation.

3.3 Cool-down

During cool-down, the engine is assumed to consume no fuel and generate no heat. Auxiliary electrical systems in the engine may require additional power to complete the shutdown, however. Thus:

$$\begin{aligned} P_{net} &= P_{net,cool-down} \\ Q_{gen,ss} &= 0 \\ \dot{m}_{fuel} &= 0 \end{aligned} \quad \text{(III-27)}$$

where $P_{net,cool-down}$ (W) is the power used by the unit's control systems while in standby operation. The user prescribes a cool-down time, $t_{cool-down}$ (s) defining the duration of the cool-down period. During this period, the model's thermal response is then characterized by solving Equations III-10 and III-11.

Table III-2: Operating mode progression

Current mode	Future mode
Standby	Warm-up
Warm-up	Normal operation
Normal operation	Cool-down
Cool-down	Standby

3.4 Switching between operating modes

The model must track which operating mode the cogeneration unit is currently in and switch the unit between modes depending on the prevailing system state, control signals and plant boundary conditions. The model must switch between modes in the order prescribed in Table III-2.

The standby and normal operating modes persist for indefinite periods of time, until the unit is either activated or deactivated, respectively. The warm-up mode persists until the engine temperature exceeds its nominal value on SE devices, or in the case of ICE devices, until the specified warm-up period lapses. The cool-down mode generally persists until the specified cool-down period lapses. Gähler (2006) suggests two different treatments for the cool-down mode:

- In the *mandatory cool-down* configuration, the model must complete the cool-down period before it can be re-activated.
- In the *optional cool-down* configuration, the model will complete the cool-down period before switching to standby. However, if the model is reactivated during the cool-down period, it may immediately switch into warm-up mode.

Developers are cautioned that the intermediate operating modes (warm-up and cool-down) may span several simulation time steps, and that the transition between modes may not coincide with the start of a new time-step. Model implementations should track the system operating mode using methods consistent with the building simulation environment into which they are integrated. For example, developers might choose to i) characterize all operating modes that occur during the span of a time-step and average these values, or ii) assume that the system operates in the same mode for the duration of a time-step, and choose a sufficiently short time step to accurately characterize the transitions between modes.

4 Control interfaces

Gähler (2004) and Kelly (2004) aggregate micro-cogeneration system controls in to two categories:

- *Internal, or low-level controls* manage the operation of subsystems within the unit to achieve optimum (and safe) performance for a given operating point.
- *External, or high-level controls* manage the operation of the unit as a whole in response to conditions in the building.

4.1 Low-level controls

The cogeneration system's low level controls ensure that the optimum performance is achieved for a given set of operating conditions, and that the unit's safe range of operation is not exceeded. Not all low-level controllers are relevant in the context of building simulation. For instance, the Solo Stirling 161 and Whisper Tech SE-based cogeneration devices use a regulator to manage the pressure of the working fluid inside the cylinders (Solo Stirling Gmbh 2003, Whisper Tech 2002). While the operating pressure has a significant effect on the thermal characteristics of the unit, these effects are aggregated into the cogeneration system model's overall electrical and thermal efficiency correlations and there is no need to model this control system.

However, some low-level controls do have a significant effect on the system's thermal behaviour. It is recommended that these control functions be implemented directly within the model. These are as follows.

4.1.1 Maximum and minimum output

The cogeneration unit's range of safe operation will be bounded by two operating points corresponding to the system's maximum and minimum output. When the unit receives a control signal from an external controller that is outside of this safe operating range, a low-level controller must take action to ensure the device is not damaged:

- If the controller requests an output exceeding the system's maximum output operating point, the system should be operated to produce its maximum output.
- If the controller requests an output less than the system's minimum output operating point, the system should be either i) operated to produce its minimum output, or ii) deactivated.

Gähler (2004) notes that certain control strategies may benefit from knowledge of the system's operational constraints. He suggests that the cogeneration system model provide an interface to high-level controllers indicating if the unit's output is limited by i) its minimum operating point, or ii) its maximum operating point.

4.1.2 Overheating protection

Additional low-level controls are used to deactivate the unit when dangerous operating conditions are detected. Fault protection controls relevant in building simulation include:

- *Low cooling water flow rate:* If the flow rate of cooling water supplied to the unit is too low, the system may overheat and must be deactivated.

High cooling water temperature: If the temperature of the cooling water is too high, the system may overheat and must be deactivated. In the Solo Stirling 161 and Whisper Tech SE-based cogeneration systems, the temperature at the unit's cooling water outlet is monitored.

4.2 High-level controls

High-level controllers manage the unit's operation in response to conditions inside the building. Some ICE and SE cogeneration devices are compatible with third-party high-level controllers typically used in building applications, while others feature integrated, on-board high-level controllers, and are not readily compatible with third-party products. To preserve the flexibility of the proposed model, it is recommended that all high-level controllers be implemented as external modules, even if they represent control systems that are fully integrated into cogeneration devices.

The cogeneration system model specification provides two interfaces to the high-level control modules, permitting them to set the cogeneration system operating point without knowledge of the configuration or operation of the device. Data received by the model through these interfaces can be mapped to one or more key model parameters, and used to uniquely determine the requested operating point.

The two interfaces proposed are: i) an electrical demand interface, and ii) a dimensionless control signal interface:

Electrical control interface: The controller will provide the electrical control interface with a desired electrical power flux P_{demand} (W). The cogeneration system model will determine the operating point corresponding to this power output ($P_{net,ss}=P_{demand}$).

Dimensionless control signal interface The controller will provide the dimensionless control signal interface with a value, u, that varies between 0 and 1. The cogeneration system model will map this signal to a controllable parameter, such that the system's maximum operation point is achieved when u=1, and the minimum operating point is achieved when u=0. Setting u to a value less than zero will cause the system to be deactivated. The steady-state power output is the most suitable parameter for use with the dimensionless control signal:

$$P_{net,ss} = P_{net,min} + u(P_{net,max} - P_{net,min}) \qquad \text{(III-28)}$$

The unit operating point may differ from the steady-state value requested by the external controllers due to the dynamic effects discussed previously..

4.2.1 Control flags

In addition to the control signal, the controller should provide to the cogeneration model a flag indicating if the unit should be activated, and which control interface is in use. This flag should support three states:

- deactivate the unit
- activate the unit and use the electric load following interface
- activate the unit and use the dimensionless load following interface

The control flag is only necessary when both the dimensionless or electric control signal interfaces are implemented. Implementations making exclusive use of either interface may choose to omit the control flag, and assume that the unit switches to standby when a control signal of zero (or less) is received.

4.2.2 Additional data output

Gähler notes that some control strategies may benefit from knowledge of the unit's operating constraints. To support these controls, the model must indicate:

- if the unit's fuel flow is constrained by its maximum or minimum rate of change,
- if the unit's electrical output is constrained by its maximum or minimum rate of change, and
- if the calculated, steady-state rate heat generation ($q_{ss,gen}$) differs significantly from the rate of heat transfer to the cooling water (q_{HX}).

5 Emissions

The model specification provides a rudimentary emission model for performing the carbon dioxide emission calculations required in the Annex 42 performance assessment work. A pragmatic model for the emissions of trace elements such as CO, NO_X and SO_X is also proposed, but its implementation is not essential for Annex 42's objectives

5.1 CO_2 Emissions

The model specification provides a CO_2 emission model that assumes complete combustion of the hydrocarbon fuel:

$$\dot{m}_{CO_2} = \left(\frac{\dot{m}_{fuel}}{\sum_{fuel\ constituents} \chi_i MM_i} \right) \left(\sum_{fuel\ constituents} \chi_i n_{C,i} \right) MM_{CO_2} \qquad \text{(III-29)}$$

where $\dot{m}_{CO_2}$ is the mass flow rate of CO_2 emitted by the unit, χ_i is the fraction of fuel constituent *i*, MM_i is the molar mass of fuel constituent *i*, $n_{C,i}$ is the number of mols of carbon in a single mol of constituent *i*, and MM_{CO_2} is the molar mass of CO_2.

5.2 Trace emissions

A useful capability in any heat and power source model is the ability to map performance to trace emissions such as CO, NO_X and SO_X. In more complex engine models this is achieved by detailed modelling of the combustion process. However for the model described here a more pragmatic solution is proposed through the use of empirically derived "fuel emissions coefficients". So, for example the CO emissions rate (kg/s) for the cogeneration system would be determined by:

$$\dot{m}_{CO} = \dot{m}_F e_{CO} \qquad \text{(III-30)}$$

where e_{CO} is the CO emissions coefficient (kg CO/kg fuel).

Similar coefficients can be derived from experimental results for other pollutants such as NO_x, SO_x and particulates. Note the use of a fixed coefficient neglects the fact pollutant emissions will be more pronounced during the engine start up period, when the engine is operating while relatively cold resulting in very poor efficiency, high fuel consumption and consequently high emissions. One mechanism of dealing with this problem is to include fuel consumption and emissions coefficient modifiers, which are a function of time, and which attain a value of 1 when the engine unit has warmed up. For example the fuel consumption rate (kg/s) of the ICE engine during the cold start up period would therefore be:

$$\dot{m}_{CO_2} = \dot{m}_F e_{CO}\, \lambda(t) \qquad \text{(III-31)}$$

where t is the present time (s). One possible form of the time-varying modifier is an exponential decay function:

$$\lambda(t) = e^{-(t-t_o)/\tau} \qquad \text{(III-32)}$$

where τ is an empirically derived time constant (s) and t_o is the unit start time (s).

Naturally the determination of the time varying modifier λ (-) would require the monitoring of electrical loading, fuel consumption and exhaust gas composition over a start up period — requiring considerable experimental effort.

6 Model Architecture

The state equations and empirical correlations characterizing the cogeneration system model are summarized in Table III-2. The model has three environmental boundary conditions that are determined elsewhere in the simulation environment:

- surrounding air temperature,
- cooling water temperature, and
- cooling water mass flow rate.

In addition, the model has a fourth boundary condition provided by the external controller. This condition is either the steady-state electrical output requested by the controller or a dimensionless control signal, depending on which control interface described in Section 4 is in use.

The model solution procedure is depicted in Figure III-2. Under most circumstances, the model can be explicitly solved. However, if the rate of change in the fuel flow rate is found to exceed empirically derived constraints, the system's operating point (ie $P_{net,ss}$) must be adjusted and the solution repeated. Well-known procedures such as Newton's method and the bisection method may be used to ensure fast and accurate convergence of the iteration (Kreyszig 1993).

7 Conclusions

This specification describes the basic form for a generic combustion-based engine micro-cogeneration model for use in building simulation. The modelling approach used in this work relies on empirically-derived correlations to characterize device-specific performance coupled with a mechanistic approach to represent dynamic heat transfer between the unit and balance of plant components. This specification has evolved from higher resolution models developed independently for both internal combustion and Stirling engine cogeneration systems, both of which were deemed impractical given the input/output measurements available from Annex 42 experimental work.

While this model specification has been developed for ICE and SE-based cogeneration technology, the result is a generalized cogeneration system model that can be used to study any device providing both heat and electricity by oxidizing a hydrocarbon fuel. The model is well-suited for use in Annex 42 — the data requirements are consistent with the experiments being performed by Annex 42 participants, and its structure is sufficiently simple for incorporation into building simulation software.

Annex 42 is also developing detailed models of cogeneration systems based on hydrocarbon-fueled proton-exchange membrane and solid oxide fuel cell technology for use in building simulation. While the inner workings of these devices differ significantly from those of the ICE and SE-based cogeneration units, the cogeneration system model proposed in this specification is arguably applicable to fuel-cell based technology as well. Future work contrasting the predictions of this generalized model and the dedicated fuel cell models would prove very interesting, and might guide future heat and power source model development.

Table III-2: Summary of cogeneration system model equations

$\eta_e = f(\dot{m}_{cw}, T_{cw}, P_{net,ss})$	Steady-state net electrical efficiency
$\eta_q = f(\dot{m}_{cw}, T_{cw}, P_{net,ss})$	Steady-state cogeneration efficiency
$q_{gross} = P_{net,ss} / \eta_w$	Gross heat input
$q_{gen,ss} = \eta_q q_{gross}$	Steady-state heat output
$\dot{N}_{fuel} = q_{gross} / LHV_{fuel}$	Fuel flow rate
$\dot{m}_{fuel}^{t+\Delta t} = \begin{cases} \dot{m}_{fuel,demand}^{t+\Delta t} & \text{if } d\dot{m}_{fuel}/dt \le \left(d\dot{m}_{fuel}/dt\right)_{max} \\ \dot{m}_{fuel}^{t} \pm \left(d\dot{m}_{fuel}/dt\right)_{max} & \text{if } d\dot{m}_{fuel}/dt > \left(d\dot{m}_{fuel}/dt\right)_{max} \end{cases}$	Dynamic fuel input
$\dot{m}_{air} = f(P_{net,ss})$	Combustion air flow
$P_{net}^{t+\Delta t} = \begin{cases} P_{net,ss}^{t+\Delta t} & \text{if } dP_{net}/dt \le \left(dP_{net}/dt\right)_{max} \\ P_{net}^{t} \pm \left(dP_{net}/dt\right)_{max} & \text{if } dP_{net}/dt > \left(dP_{net}/dt\right)_{max} \end{cases}$	Dynamic power output
$[MC]_{sys} \frac{dT_{sys}}{dt} = UA_{HX}\left(T_{cw,o} - T_{sys}\right) + UA_{loss}\left(T_{room} - T_{sys}\right) + q_{gen,ss}$ $[MC]_{cw} \frac{T_{cw,o}}{dt} = [\dot{m}c_p]_{cw}\left(T_{cw,i} - T_{cw,o}\right) + UA_{HX}\left(T_{sys} - T_{cw,o}\right)$	Dynamic heat recovery

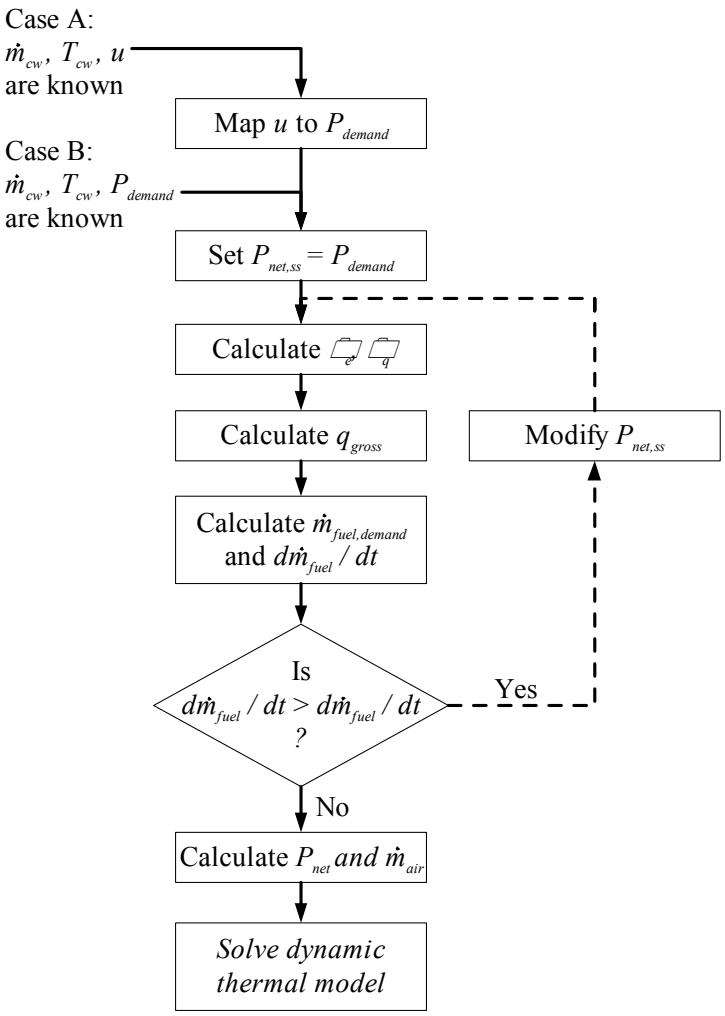

Figure III-2: cogeneration model solution procedure

8 References

Abd Alla, G H. 2002. *Computer simulation of a four stroke spark ignition engine*, Energy Conversion and Management, 43, pp 1043-106.

Annand W J D, 1963, Heat transfer in the cylinders of reciprocating internal combustion engines, Proc. Inst. Mech. Engineers, 177:973-990

Bell, M., Swinton, M., Entchev, E., Gusdorf, J., Kalbfleisch, W., Marchand, R. Szadkowski, F. 2003. , Development of micro combined heat and power technology assessment capability at the Canadian Centre for Housing Technology, draft final report, Technical report, National Research Council Canada, and Natural Resources Canada.

Braun J E, Klein S A, Mitchell J M, 1989, "Effectiveness Models for Cooling Towers and Cooling Coils", ASHRAE Transactions, 95(2).

Beausoleil-Morrison I, 2005, Model specifications for an SOFC cogeneration device, IEA Annex 42 draft internal report.

Clarke J A, 2001, Energy simulation in building design, Butterworth Heineman, 2nd edition.

Costea, M., Petrescu, S. Harman, C. 1999 , 'The effect of irreversibilities on solar Stirling cycle performance', Energy Conversion and Management 40, 1723–1731.

Dentice d'Accadia M, Sasso M, Sibilio S, Vanoli L, 2003, "Micro-combined heat and power in residential and light commercial applications", Applied Thermal Engineering, 23 (10) 1247-1259

Dochat, G. 1993. , SPDE/SPRE final summary report, Technical report, Mechanical Technology Incorporated.

Ferguson, A. 2004. , Inventory of empirical data suitable for validation of cogeneration models, IEA/ECBCS Annex 42 Subtask B working document, Natural Resources Canada.

Ferguson A, 2005, Stirling Engine model specifications, IEA Annex 42 draft internal report.

Gähler, C. 2004. , Review of SOFC, PEMFC, Stirling and ICE model specifications, Technical report, Siemens Building Technologies. IEA/ECBCS Annex 42 working document.

Gähler, C. 2006. Email communication of March 21, 2006.

Griffith, B. 2006. Email communication of June 19, 2006.

Henckes, L. Stripf, M. 2003. , Laboratory test of the SOLO Stirling CHP module, Technical report, European Institute for Energy Research.

Heywood J B, 1998, Internal Combustion Engine Fundamentals, McGraw Hill.

Honda 2004, Micro CHP product presentation.

Hrovat D, Sun J, 1997, Models and control methodologies for IC engine idle speed control design, Control Engineering Practice, 5 (8), 1093-1100.

Hsu, Lin Chiou2003Hsu03 Hsu, S., Lin, F. Chiou, J. 2003 , 'Heat-transfer aspects of stirling power generation using incinerator waste energy', Renewable Energy 28, 59–69.

Kays and London, Compact Heat Exchangers, 1964, 2nd Ed, McGraw Hill.

Kelly, N. 2004a. , Specifications for models of cogeneration equipment: discussion document, IEA/ECBCS Annex 42 Subtask B working document, University of Strathclyde.

Kelly N J, 2004b, Review of small scale cogeneration system models, IEA Annex 42 draft internal report

Kelly N J, 1998, Towards a design environment for building-integrated energy systems: the integration of electrical power flow modelling with building simulation, PhD thesis, University of Strathclyde.

Knight, I. Ugursal, V. 2004. , Residential cogeneration systems: A review of the current technologies, Technical report, International Energy Agency: Energy in Buildings and Community Systems Annex 42.

Kreyszig, E. 1993 , Advanced Engineeing Mathmatics, seventh edn, John Wiley and Sons, Inc.

Larminie, J. and Dicks, A. 2001. Fuel cell systems explained, John Wiley and Sons Inc.

McCrorie KAB, Underwood W B, le Feuvre R F, 1996, Small-scale combined heat and power simulations: development of a dynamic spark-ignition engine model, Building Services Engineering Research and Technology, Vol 17, No. 3.

Pearce, J., Al Zahawi, B., Aukland, D. Starr, F. 1996 , 'Energy generation in the home: evaluation of single-house domestic combined heat and power', IEE Proceedings of Science, Measurement and Technology 143(6), 345–350.

Pearce, J., Al Zahawi, B. Shuttleworth, R. 2001 , 'Energy generation in the home: modelling of single-house domestic combined heat and power', IEE Proceedings of Science, Measurement and Technology 148(5), 197–203.

Qin X, Chen L, Sun F and Wu C, 2003 The universal power and efficiency characteristics for irreversible reciprocating heat engines, European Journal of Physics, 24 359-366.

Schreiber, J., Geng, S. Lorenz, G. 1986. , RE-1000 free-piston stirling engine sensitivity test results., Technical report, National Aeronautics and Space Administration.

Solo Stirling GmbH 2003. , 'Solo Stirling 161 combined power/heat-module: technical documentation', Technical specifications. Version 1.9, available on Solo's website: http://www.stirling-engine.de/engl/TecDoc.v-1.9_GB.pdf.

Urieli, I. Berchowitz, D. 1984 , Stirling cycle analysis, Adam Hilger Ltd. Bristol.

Weber, A. 2004. , IEA Annex 42 Stirling model specifications (review), Technical report, EMPA. IEA/ECBCS Annex 42 working document.

Whisper Tech Ltd. 2002. , WhisperGen Installation Manual: Model PPS24-ACLG, Whisper Tech Ltd., P.O. Box 13-705, Christchurch New Zealand.

Zilch, R. 2005, Presentation on SenerTec ICE CHP unit at IEA/ECBCS Annex 42 meeting in Munich, September.